Neuropeptidergic circuit modulation of developmental sleep in *Drosophila*

Chikayo Hemmi[1], Kenichi Ishii[1, #], Mana Motoyoshi[1], Masato Tsuji[1] and Kazuo Emoto[1, 2, #, $]

[1]Department of Biological Sciences, The University of Tokyo

[2]International Research Center for Neurointelligence (WPI-IRCN), The University of Tokyo

[#]Corresponding authors

[$]Lead contact: emoto@bs.s.u-tokyo.ac.jp

Abstract

Sleep-wakefulness regulation dynamically evolves along development in a wide range of organisms. While the mechanism regulating sleep in adults are relatively well understood, little is known about its counterpart in early developmental stages. Here we report a neuropeptidergic circuitry that modulates sleep in developing *Drosophila* larvae. Through an unbiased screen, we identified the neuropeptide Hugin and its receptor PK2-R1 as critical regulators of larval sleep. Our genetic and behavioral data suggest that HugPC neurons secrete Hugin peptides to activate Insulin-producing cells (IPCs), which expresses a Hugin receptor PK2-R1. IPCs, in turn, release insulin-like peptides (Dilps) to regulate sleep. We further show that the Hugin/PK2-R1 axis is dispensable for adult sleep. Our findings thus reveal the neuromodulatry circuit that regulates developmental sleep in larvae, and highlight differential impacts of the same modulatory axis on early-life sleep and adult sleep.

Introduction

Sleep is a fundamental state with significant impacts on many aspects of cognition and metabolism (Blumberg et al., 2005; Davis et al., 2004; Sorribes et al., 2013). While sleep remains essential throughout life, its regulation dynamically unfolds over the course of development. For instance, the pace of sleep-wakefulness cycle is relatively fast in infants, while gradually slows down and stabilize in adults (Blumberg et al., 2005; Davis et al., 2004; Sorribes et al., 2013). Furthermore, sleep-wake cycle in infants is typically independent of circadian rhythm, but it gradually comes under the circadian regulation (Davis et al., 2004; Frank et al., 2017; Poe et al., 2023). Such developmental evolution of sleep-wakefulness cycles appears to be conserved across a wide range of organisms including flies, fishes, mammals and humans (Blumberg et al., 2005; Davis et al., 2004; Poe et al., 2023; Sorribes et al., 2013; Szuperak et al., 2018a). In contrast to deep insights into the molecular and neural mechanisms underlying adult sleep regulation (Barlow & Rihel, 2017; Scammell et al., 2017; Shafer & Keene, 2021), little is known about regulatory mechanisms underlying developmental sleep in infants, partially due to a lack of convenient models to study developmental sleep.

Drosophila larvae have recently emerged as a suitable model to study sleep regulation mechanisms. Recent studies have reported that the second instar larvae show short periods (< 6 seconds) of "inactive state" during locomotion. Importantly, such "inactive state" is consistent with the general definition of sleep: reduced responsiveness to noxious stimuli, homeostatic response to sleep deprivation, and rapid reversibility upon stimulation (Szuperak et al., 2018), suggesting that the "inactive state" in larvae likely corresponds to the sleep state. Interestingly, loss-of-function mutations in the clock genes *clock* and *cyc* fail to impact the larval sleep, while significantly altering the sleep patterns in adult flies (Dubowy & Sehgal, 2017; Hendricks et al., 2003; Szuperak et al., 2018). Likewise, mutations in the dopamine transporter *DAT* fail to influence larval sleep, while reducing sleep amounts in adult (Kume et al., 2005; Szuperak et al., 2018). These observations imply that sleep regulation mechanisms might be at least in part distinct between larvae and adults, yet the neural mechanism of larval sleep remains vastly understudied compared to that of adult sleep.

In this study, we performed an unbiased genetic screen in the second instar larvae, and identified the neuropeptide Hugin and its receptor PK2-R1 as a pair critical for larval sleep. At the circuit level, Hugin-producing HugPC neurons directly stimulate the insulin-producing cells (IPCs) via PK2-R1 to regulate sleep. We further found that regulators of larval sleep are either irrelevant or exert the opposite effects on adult sleep. Overall, our findings uncover the neuropeptidergic circuitry that regulates developmental sleep in larvae, and highlight mechanistic differences between larval and adult sleep.

Results

PK2-R1 is required for wake/sleep control in Drosophila larvae

To understand molecular and neural mechanisms of larval sleep, we modified a previously reported system (Churgin et al., 2019; Szuperak et al., 2018) to automatically quantify the sleep amount of second instar larvae (Figure 1-figure supplement 1A-1C) (see Materials & Methods for details). Our system automatically annotates larvae in each frame as

either “inactive” or “active” states on the basis of pixel changes, with ~90% accuracy compared to manual annotation (Figure 1-figure supplement 1C; see Methods for details). We found that bouts of ≥ 12 inactive frames are consistent with the general criteria for sleep; reduced responsiveness to noxious stimuli, homeostatic response to sleep loss, and rapid reversibility upon stimulation (Raizen et al., 2008; Szuperak et al., 2018) (Figure 1-figure supplement 2B–D). Therefore, the present study defines sleep as inactive state of ≥ 12 consecutive frames (Figure 1-figure supplement 1A).

Using this system, we next carried out an unbiased screen for genes involved in sleep regulation. To this end, we tested 47 CRISPR knock-out lines of genes encoding enzymes or receptors for neuropeptides and monoamines (Deng et al., 2019)(Supplemental Table 1). As illustrated in Figure 1-figure supplement 3, 13 out of 47 homozygous null mutants exhibited significant changes in sleep amounts compared to the control group. To further test the functions of these candidate genes, we next took advantage of the CRISPR knock-in drivers in which GAL4 sequence is inserted into each gene locus. With these drivers, we silenced neurons expressing each candidate gene by expressing the inward-rectifying potassium channel Kir2.1 (Baines et al., 2001). Silencing neurons expressing *Oamb* and *PK2-R1* resulted in significant sleep increase, phenocopying the knock-out of these genes (Figure 1A and 1B and Figure 1-figure supplement 4D). *Oamb* encodes the octopamine receptor and has been reported to be involved in larval sleep (Szuperak et al., 2018). The role of PK2-R1 in larval sleep, on the other hand, has been unknown to date. Given its strong expression in insulin-producing cells (Schlegel et al., 2016) and its function as a receptor for the neuropeptide Hugin, which modulates feeding (Schoofs et al., 2014), we hypothesized that PK2-R1 might mediate neuropeptidergic signaling that links metabolic and sleep regulation during development. We thus focused on this gene as a candidate connecting behavioral and endocrine sleep control.

Insulin-producing cells express PK2-R1 and regulate sleep states in developing larvae

Since the *PK2-R1* driver broadly labeled neurons (~1000 cells) throughout the CNS (Figure 1C), we next attempted to identify a subpopulation of these neurons relevant for

114 sleep regulation. To narrow down the candidates within PK2-R1-positive populations,
115 we examined subsets labeling GABAergic, cholinergic, or glutamatergic neurons, as
116 well as those co-expressing other neuropeptides identified in our screen, but none of
117 these manipulations reproduced the sleep phenotype caused by PK2-R1 perturbation.
118 Notably, insulin-producing cells (IPCs) in the pars intercerebralis (PI), the
119 neurosecretory center of *Drosophila*, have been reported to express *PK2-R1* (Schlegel et
120 al., 2016). Consistently, the *PK2-R1*$^{2A\text{-}LexA}$ knock-in driver labeled all IPCs (Figure 2A
121 and B). To assess whether IPCs are involved in larval sleep, we silenced IPCs with
122 Kir2.1 expression, using the IPC-specific drivers *Dilp3*- and *Dilp5-GAL4* (Figure 2C).
123 We found that silencing of IPCs significantly increased the sleep amounts compared to
124 the control, phenocopying *PK2-R1* neuron silencing and *PK2-R1* knockout (Figure 1A).
125 Consistently, both *Dilp3* and *Dilp5* null mutants exhibited larger sleep amounts
126 compared to the control (Figure 2D). These phenotypes of *Dilp* mutants and IPC
127 silencing are unlikely to be accounted for by locomotion defects, as the travel distances
128 during wake periods were unaffected (Fig. 2—figure supplement 1). Through these
129 trials, insulin-producing cells (IPCs) emerged as one of the populations whose silencing
130 phenocopied PK2-R1 loss, supporting their key role in larval sleep regulation while not
131 excluding contributions from other PK2-R1-expressing neurons. Collectively, these
132 findings suggest that *PK2-R1* in IPCs regulates larval sleep.
133
134 **Hugin-expressing neurons control larval sleep states**
135 Given that PK2-R1 is a receptor of the neuropeptide Hugin (Rosenkilde et al., 2003), we
136 next examined whether Hugin is involved in the larval sleep. We found that *Hug* mutant
137 larvae exhibited significantly larger sleep amounts compared to the control (Figure 3A),
138 consistent with *PK2-R1* knockouts (Figure 1A). When we silenced Hug-expressing
139 neurons by driving the expression of Kir2.1 with the *Hug* CRISPR-knock-in driver
140 *Hug*$^{2A\text{-}GAL4}$ (Deng et al., 2019), it resulted in a significant increase of sleep amounts
141 without detectable changes in locomotion speed (Figure 3B and Figure 3—figure
142 supplement 1B). Conversely, activation of *Hug*-expressing neurons with the red-shifted
143 channel rhodopsin ReaChR (Inagaki et al., 2014) or heat-sensitive ion channel TrpA1
144 (Hamada et al., 2008) both caused a significant reduction of sleep amount (Figure 3C
145 and D) and increased locomotor activity. However, locomotion changes were not

146 consistently observed upon either activation or suppression of Hug neurons (Figure 3—
147 figure supplement 1), suggesting that changes in sleep cannot be simply explained by
148 locomotor alterations. We further quantified larval feeding using a dye-based ingestion
149 assay and found that silencing HugPC neurons reduced food intake (Figure 3—figure
150 supplement 3), indicating that the sleep phenotype is unlikely to be explained by
151 feeding behavior being misclassified as sleep. These data together indicate that *Hug*-
152 expressing neurons are responsible for downregulating larval sleep.
153
154 *Hug*-expressing neurons are comprised of 20 cells in the subesophageal zone (SEZ) of
155 the brain, and are classified into four subpopulations based on their projection patterns
156 (Bader et al., 2007). Of these, one subpopulation called HugPC neurons (Bader et al.,
157 2007) have been reported to form synaptic connections with IPCs (Hückesfeld, Peters,
158 & Pankratz, 2016). We thus suspected that HugPC neurons may be responsible for sleep
159 regulation. In line with this notion, axons of HugPC neurons, labeled by a newly
160 generated *HugPC-LexA* driver (Figure 3—figure supplement 2), and IPCs, labeled by
161 *Dilp3-GAL4* (Figure 3E), exist in space close to each other. Indeed, silencing of HugPC
162 neurons by Kir2.1 significantly increased larval sleep (Figure 3F), phenocopying those
163 observed in *Hugin* and *PK2-R1* mutants. These results hint at the possibility that HugPC
164 neurons activate IPCs via Hugin/PK2-R1 signaling to regulate sleep.
165
166 **Hugin triggers Ca^{2+} elevation and Dilp secretion in larval IPCs via PK2-R1**
167 A previous report showed that IPCs exhibit increased firing rates and intracellular
168 calcium (Ca^{2+}) levels upon stimulation (Kréneisz et al., 2010). This motivated us to next
169 test if Hugin activates IPCs. To further visualize the output pattern of HuginPC neurons,
170 we expressed the presynaptic marker Syt-eGFP in HuginPC neurons (Figure 4—figure
171 supplement 1).To test whether Hugin activates IPCs, we utilized the recently developed
172 calcium indicator CRTC::GFP, which can report Ca^{2+} dynamics in the timescale of
173 several minutes (Bonheur et al., 2023). As glucose reportedly triggers Ca^{2+} dynamics in
174 IPCs in a range of minutes (Oh et al., 2019), we wondered if CRTC::GFP can detect this
175 dynamics, as a positive control. To this end, we applied D-glucose to isolated larval
176 brains and found a significant cytosol-to-nuclear translocation of CRTC::GFP in IPCs
177 within ~5 min, confiming that this reporter can indeed detect Ca^{2+} responses in IPCs

178 upon stimulation (Figure 5B). We then examined whether *Hug* neurons act upstream of
179 *PK2-R1*-expressing IPCs by measuring Ca^{2+} responses of IPCs while thermogenetically
180 activating *Hug* neurons with TrpA1. We found that activation of *Hug* neurons tended to
181 increase Ca^{2+} levels in IPCs (Figure 4B and C), consistent with the HuginPC-to-IPCs
182 axis (Figure 4D). Next, we tested whether Hug peptides can induce Ca^{2+} responses in
183 IPCs using *ex vivo* preparations. The *Hug* gene encodes a precursor that potentially
184 produces at least two distinct peptides, Hug-γ and PK-2, both of which can bind PK2-
185 R1 to induce Ca^{2+} responses (Rosenkilde et al., 2003). We thus incubated the
186 CRTC::GFP-expressing larval brain with chemically synthesized Hug-γ or PK-2
187 (Kréneisz et al., 2010; Oh et al., 2019) (Figure 5A). We found that bath application of
188 either Hug-γ or PK-2 induced significant Ca^{2+} responses in IPCs (Figure 5B–D). In
189 agreement with the idea that Hug peptides activate IPCs via *PK2-R1*, knock-out of *PK2-*
190 *R1* blocked the Hug peptide-evoked Ca^{2+} elevations in IPCs (Figure 5F and G). Similar
191 results were obtained when we bath-applied the synthetic Neuromedin U (NMU), the
192 mammlaian homlog of Hugin (Figure 5A and 5G), suggesting the role of Hugin/PK2-
193 R1 signaling may be conserved across species. Furthermore, Dilp3 accumulated in IPCs
194 were significantly reduced after applying Hug peptides, suggesting that Hugin causes
195 IPCs to release Dilp3 (Figure 5E). Collectively, these data suggest that *Hug* neurons
196 activate IPCs via the Hug/PK2-R1 signaling to regulate sleep (Figure 5H).
197
198 **Hugin/PK2-R1 axis has distinct impacts on wake/sleep control in larvae and adults**
199 Given the differences between larval vs adult sleep in temporal pattern and circadian
200 influence, we next wondered if Hug/PK2-R1/Dilps axis functions in adult sleep as well.
201 As in larvae, *PK2-R1* knockout adults showed increased sleep amount compared to the
202 control (Figure 6—figure supplement 1B). In contrast, *Hug* knockout or silencing of
203 HugPC neurons failed to influence adult sleep (Figure 6A and 6B). This suggests that,
204 unlike larvae, Hug is dispensable for adult sleep. Interestingly, we observed that the
205 expression patterns of PK2-R1 and Hug, and the morphology of HugPC neurons and
206 IPCs, showed a broadly similar distribution in larvae and adults, although we did not
207 directly track individual neurons across development (Figure 6—figure supplement 2).
208 This implies that the differential roles of Hug in larvae vs adults are likely due to
209 physiological differences in HugPC neurons and/or IPCs. We thus examined how Hug

210 peptides evoke Ca^{2+} responses in adult IPCs and found that neither Hug-γ nor PK-2
211 could induce Ca^{2+} responses in adult IPCs (Figure 6D and 6E), unlike in larvae.
212 Although PK-2 treatment even led to a modest increase in Dilp3 immunoreactivity in
213 adult IPCs (Figure 6F), the physiological significance of this effect remains unclear; at
214 present, we consider it most likely that PK-2 acts on larval and adult IPCs in a different
215 manner. These data indicate that Hug induces Ca^{2+} responses and Dilps secretion in
216 larval IPCs but not in adult IPCs. Surprisingly, we further found that *Dilp3* or *Dilp5* null
217 mutations reduced sleep amounts in adults, consistent with previous reports (Cong et al.,
218 Sleep 2015) (Figure 6C), while in larvae, these mutations in fact increased the sleep
219 amounts. These data unexpectedly reveal how the same set of neuronal circuits and
220 molecular signaling therein can evolve over development in a complex manner.
221

222 **Discussion**

223 In this study, we have identified the neuropeptide Hugin and its receptor PK2-R1 as a
224 ligand/receptor pair critical for sleep regulation in *Drosophila* larvae. We have further
225 shown that larval IPCs express PK2-R1, respond and release Dilp3 upon Hugin
226 stimulation. Surprisingly, the Hugin/PK2-R1 axis is dispensable for sleep regulation in
227 adults, even though the gene expressions as well as the circuit structure appeared to be
228 conserved between larval and adult brains. Furthermore, Dilps appear to modulate sleep
229 in opposite directions in larvae and adults. Our findings thus uncover the
230 neuropeptidergic modulation circuitry that specifically regulates developmental sleep,
231 and suggest divergent usage of the same molecules and circuitry for sleep modulation in
232 larvae and adults.
233

234 **Hugin/PK2-R1/Dilps axis negatively regulates sleep in larvae**

235 The present study shows that the neuropeptide Hugin and its receptor PK2-R1 are
236 required for sleep regulation in the early larval stage. This notion is supported by
237 following lines of evidence. First, knock-out mutations in *Hugin* or *PK2-R1* increased
238 sleep amounts compared to the control (Figure 1A and 3A). Consistently, silencing a
239 subpopulation of *Hugin*-expressing neurons, called HugPC neurons, or *PK2-R1* neurons
240 increased sleep amounts (Figure 1B, 3B and 3F). Second, thermogenetic activation of

241 Hugin neurons decreased sleep amounts (Figure 3D). Third, HugPC neurons project
242 their axons to IPCs in the brain that express PK2-R1 receptors (Figure 3E). Fourth,
243 Hugin peptides induced Ca^{2+} elevation and promoted Dilp3 release from IPCs in a PK2-
244 R1-dependent manner (Figure 5). Last, *Dilp3* null mutations increased sleep amounts
245 (Figure 2D). Based on these data, we propose a model in which the Hugin/PK2-
246 R1/Dilps axis along the HugPC-IPC circuitry modulates larval sleep (Figure 7).
247
248 Examples of Hugin acting through PK2-R1 are prominent in the context of feeding
249 regulation in larvae and adults (Schoofs et al., 2014). For example, a recent study has
250 suggested that Hugin regulates the timing of pupariation and body wall contraction
251 during pupariation through PK2-R1 in PTTH neurons (Ohhara et al., 2024). In the
252 present study, we showed that HugPC in the larval brain modulates sleep (Figure 3F). A
253 previous electron microscopic analysis suggested that larval HugPC neurons likely form
254 synaptic connections to downstream neurons including IPCs (Hückesfeld et al., 2021;
255 Schlegel et al., 2016). We here showed that PK2-R1 is required for larval sleep control
256 and that thermogenetic activation of Hug neurons is associated with Ca^{2+} responses in
257 PK2-R1-expressing IPCs *in vivo* (Figure 4). Importantly, our *ex vivo* data indicated that
258 Hugin peptide-induced Ca^{2+} response in IPCs was largely abolished by *PK2-R1*
259 mutation (Figure 5), indicating the critical role of the Hugin/PK2-R1 axis for the
260 HugPC-mediated IPC activation. Together, we propose that the HugPC-IPCs circuity
261 mobilizes Hugin/PK2-R1 signaling to selectively modulate larval sleep. Interestingly,
262 our *ex vivo* data indicated that Neuromedin U (NMU), a mammalian ortholog of Hugin,
263 can trigger Ca^{2+} responses in larval IPCs in a PK2-R1-dependent fashion (Figure 5).
264 Given that NMU has been implicated in sleep regulation in fishes and mammals
265 (Ahnaou & Drinkenburg, 2011; Chiu et al., 2016), an analogous ligand/receptor pair
266 might be involved in sleep modulation in mammals as well.
267
268 In this study, activation of Hugin–PK2-R1 signaling by bath application of Hugin
269 peptides led to a significant reduction in Dilp3 immunoreactivity in IPCs, whereas
270 Dilp2 immunoreactivity did not show a decrease under these conditions, suggesting that
271 Hugin–PK2-R1 activation promotes Dilp3 secretion without strongly enhancing Dilp2
272 release in our assay. One plausible explanation is that individual Dilps are stored in

273 partially distinct vesicular pools within IPCs and are released through stimulus-specific
274 mechanisms. Consistent with this idea, previous work has shown that Dilp release from
275 IPCs can be selective, with Dilp2 and Dilp3 responding to distinct nutritional cues (Kim
276 and Neufeld, 2015). Confocal analyses in that study further demonstrated that Dilp2 and
277 Dilp3 segregate into different intracellular granules, supporting the notion that
278 individual Dilps can be targeted to distinct secretory pathways within the same neurons.
279 In light of these observations, the selective effect of Hugin–PK2-R1 activation on
280 Dilp3, but not Dilp2, is readily interpreted as another example of non-uniform Dilp
281 regulation. Rather than uniformly driving secretion of all IPC-derived Dilps, we propose
282 that Hugin–PK2-R1 signaling preferentially mobilizes the Dilp3 secretory pathway.
283 Such selective regulation is reminiscent of piecemeal degranulation in mammalian
284 eosinophils and mast cells, as well as stimulus-dependent mobilization of specific
285 vesicle pools in pancreatic β cells. In this model, different Dilps are stored in partially
286 distinct vesicular pools and are mobilized by different upstream inputs. While
287 ultrastructural approaches such as electron microscopy could provide further insight
288 into the anatomical segregation of Dilp-containing vesicles, these analyses are
289 technically beyond the scope of the present study, and we therefore highlight them as an
290 important direction for future work.
291
292 PK2-R1 knockout larvae exhibited both an increase in sleep and a reduction in
293 locomotion speed. Because our locomotor metric is defined as travel distance per unit
294 time during epochs classified as wake, the observed decrease in locomotion speed
295 cannot be fully explained by the increased fraction of time spent in sleep. Nevertheless,
296 we cannot exclude the possibility that part of the apparent sleep increase in the knockout
297 reflects broader motor impairments in PK2-R1–expressing circuits. PK2-R1 expression
298 is not confined to IPCs but is broadly distributed in the nervous system, including
299 populations in the ventral nerve cord (Figure 1C), making it likely that PK2-R1–positive
300 neurons outside IPCs contribute to locomotor control. Consistent with this idea, when
301 we restricted our manipulations to IPCs, we observed robust changes in sleep without
302 significant alterations in locomotor activity (Figure 2—figure supplement 1). These
303 findings suggest that IPCs are more directly involved in sleep regulation, whereas other
304 PK2-R1–expressing neurons may predominantly influence locomotion.

305

306 Dh44 neurons promote arousal in second-instar larvae (Poe et al., 2023), raising the
307 possibility that hugin signaling may influence sleep through Dh44 in addition to IPCs.
308 Consistent with this idea, the hugin receptor PK2-R1 is expressed not only in IPCs but
309 also in Dh44 and DMS neurons (Schlegel et al., 2016). Thus, an extension of our model
310 is that HuginPC-derived hugin may act on multiple PK2-R1–positive targets (including
311 IPCs and potentially Dh44/DMS neurons) to shape larval sleep. Future cell type-
312 specific perturbations of PK2-R1 in Dh44 and DMS neurons will be important to test
313 the contribution of these pathways.
314

315 **Divergent roles of insulin signaling in regulation of larval sleep and feeding**

316 IPCs in larvae respond to exogenously applied Hug peptides, both by exhibiting
317 elevated Ca^{2+} levels and decreases in intracellular Dilp3 storage (Figure 5C–E). In
318 contrast to Dilp3, however, the amount of Dilp2 accumulated in IPCs remains
319 unchanged following Hug peptide application (Figure 5—figure supplement 1B). On
320 the other hand, Dilp2 accumulation in IPCs decreases after glucose treatment (Figure
321 5—figure supplement 1A) (Oh et al., 2019). These results unexpectedly suggest that
322 larval IPCs form parallel channels inside, one for Hug-Dilp3 and the other for glucose-
323 Dilp2. Mechanistically, Hug acts directly on IPCs via the PK2-R1 receptor. As for
324 glucose, on the other hand, glucose-sensing CN neurons in the brain take up glucose
325 and subsequently secrete another neuropeptide to activate IPCs (Oh et al., 2019). Such
326 parallelism inside IPCs might provide insight into why insect species broadly express
327 multiple insulin-like peptide genes, in some cases even as many as 40 genes in the
328 silkworm Bombyx mori (Okamoto, 2021). Drosophila genome harbors eight Dilp genes
329 (Nässel et al., 2015), of which Dilp2, Dilp3, and Dilp5 are considered nutrient-related.
330 Nevertheless, mRNA expression or release patterns of these Dilps are not identical
331 under different nutrient conditions (Géminard et al., 2009; Kauffman & DiAngelo,
332 2024; Nässel et al., 2015; Oh et al., 2019; Tomoatsu et al., 2002). Furthermore, these
333 Dilps exhibit different binding affinities for the insulin receptor (InR), the secreted
334 decoy of InR (SDR), the ecdysone-inducible gene L2 (Imp-L2) (Okamoto et al., 2013).
335 These reports hint at the differential roles of different insulin-like peptides, but
336 mechanistic insights remain largely lacking. Our data of larval IPCs forming parallel

337 channels for Hug-Dilp3 and glucose-Dilp2 may provide a point of entry for tackling this
338 mystery.
339

340 **Differential impacts of the same neuropeptidergic modulations on larval and adult**
341 **sleep**

342 Our data show that the Hugin/PK2-R1/Dilps axis likely downregulates sleep amounts in
343 larvae. Despite the significant increase of sleep amount in *Hugin* mutant larvae, *Hugin*
344 mutant adults showed sleep amounts comparable to wild-type control (Figure 6A),
345 consistent with a previous report that Hugin is dispensable for control of baseline sleep
346 levels (Schwarz et al., 2021). According to our histological analyses, the Hugin/PK2-R1
347 expression patterns as well as the HugPC-IPCs circuitry appear to be largely conserved
348 in adults (Figure 3E and Figure 6—figure supplement 2). Unlike larval brain, however,
349 Hugin peptides failed to trigger Ca^{2+} responses in IPCs in adults (Figure 6E). It is thus
350 possible that Hugin/PK2-R1 signaling along the HugPC-IPCs circuitry is suppressed in
351 adults. IPCs in adults receive multiple positive and negative modulatory inputs through
352 GPCRs including the metabotropic $GABA_B$ receptors (Enell et al., 2010), which
353 suppresses IPC activity and Dilp release in adult IPCs (Enell et al., 2010). It is thus
354 plausible that such negative modulatory inputs to IPCs in adults might counteract with
355 the Hugin/PK2-R1 axis to suppress Dilp release. In addition, our data suggest that Dilps
356 modulate sleep amount in the opposite directions in larvae and adults (Figure 7).
357 Comparing the expression levels and activities of GPCRs in larval and adult IPCs would
358 be essential to better understand how same modulatory signals over the course of
359 development come to exert differential impacts on sleep. Interestingly, Hugin in adults
360 appears irrelevant for the baseline sleep amount but is required for homeostatic
361 regulation of sleep (Schwarz et al., 2021). Thus, testing if Hugin/PK2-R1 axis is
362 involved in the homeostatic regulation of larval sleep, and how such a system compares
363 to its adult counterpart, may further provide mechanistic insights into how homeostatic
364 sleep regulation maturates over development.
365

366 In summary, we identified the Hugin/PK2-R1/Dilps signaling along the HugPC/IPCs
367 circuit as the molecular and circuitry basis for developmental sleep regulation. Our

368 study begins to fill the knowledge gap in larval sleep regulation, and sheds light on
369 mechanistic differences in sleep regulation between early developmental stages and
370 adults.
371

372 **Materials and Methods**

373 **Fly strains**

374 The following strains of *Drosophila melanogaster* were obtained from the Bloomington
375 *Drosophila* Stock Center: *iso31* (an isogenic w^{1118} strain; BDSC# 5905), $PK2\text{-}R1^{attP}$
376 (BDSC# 84563), $PK2\text{-}R1^{2A\text{-}GAL4}$ (BDSC# 84686), $PK2\text{-}R1^{2A\text{-}LexA}$ (BDSC# 84431),
377 $Dilp3^{1}$ (BDSC# 30882), $Dilp5^{1}$ (BDSC# 30884), *Dilp3-GAL4* (BDSC# 52660), *Dilp5-*
378 *GAL4* (BDSC# 66007), Hug^{attP} (BDSC# 84514), $Hug^{2A\text{-}GAL4}$ (BDSC# 84646), $Hug^{2A\text{-}LexA}$
379 (BDSC# 84397), *UAS-Kir2.1::EGFP* (BDSC# 6596), *UAS-Stinger, LexAop-*
380 *tdTomato.nls* (BDSC# 66680), *UAS-mCD8::mCherry, UAS-CRTC::GFP* (BDSC#
381 99657), *UAS-ReaChR* (BDSC# 53741), *UAS-TrpA1* (BDSC# 26263), *LexAop-ReaChR*
382 (BDSC# 53746), *LexAop-rCD2::RFP-p10.UAS-mCD8::GFP-p10* (BDSC# 67093).
383 w^{1118} was from Y. Rao (Peking University); *HugPC-GAL4* (Hückesfeld et al., 2016)
384 was from M. Pankratz (University of Bonn); *LexAop-TrpA1* (Burke et al., 2012) was
385 from S. Waddel (University of Oxford). *HugPC-LexA* was created in this study (see the
386 following section, "Generation of transgenic lines"). Detailed lists of fly genotypes can
387 be found in the key resource table and Source Data files.
388

389 **General fly maintenance**

390 Flies were maintained in an incubator (PHCbi, model# MTR-554-PJ) set to 25°C with a
391 humidity of over 60% and a 9AM:9PM light/dark cycle. After 10 d of rearing in bottles,
392 old flies were replaced with freshly eclosed ones to maintain the strain (Furusawa et al.,
393 2023).
394

395 **Egg collection**

396 Agar substrates for egg collection were prepared by microwave-heating a mixture of 2.0
397 g sucrose (Fujifilm Wako Pure Chemicals, cat# 196-00015), 3.0 g agar (BD, cat#
398 214010), 2.5 mL apple juice (Dole), and Milli-Q water up to 100 mL. Melted agar was

399 poured into Petri dishes with a diameter of 4 cm (approximately 3 mL per dish).
400 Solidified agar was scratched with tweezers to make the surface rough. Agar plates were
401 stored inside a sealed container at 4°C. Upon egg collection, yeast paste (dried yeast
402 (Nippon Beet Sugar Co., Ltd.) kneaded with Milli-Q water at 40% (w/w)) was placed in
403 the center of the agar plates to further promote oviposition.
404
405 **Larval staging**
406 First-instar larvae were collected 2 d after egg collection. Among them, second-instar
407 larvae that molted within a 2-h window were used for video recording. Distinguishing
408 between first- and second-instar larvae was based on morphological characteristics:
409 while anterior spiracles were not evident in the first-instar, fist-shaped spiracles were
410 observed in the second-instar (Lakhotia and Ranganath, 2021).
411
412 **Larval sleep analysis**
413 Twenty-four-well silicone chambers for sleep analysis, described in Figure 1—figure
414 supplement 1, were made by pouring dimethylpolysiloxane (PDMS) into molds based
415 on a previous study (Churgin et al., 2019; Szuperak et al., 2018). As a substrate, 120 μL
416 of a mixture of 3% agar and 2% sucrose was poured into each well. After the gel
417 solidified, 10 μL per well of 60 mg/mL yeast suspension was applied to the surface of
418 the gel. Larvae were placed individually into the wells, and a glass plate (Azone, cat# 1-
419 4540-01, 5 mm × 200 mm × 200 mm) was positioned on top of the chamber to prevent
420 larvae from escaping. The chamber was placed inside a dark box equipped with a ring-
421 type infrared LED (CCS, cat# LDR2-132IR940-LA) and a camera (The Imaging
422 Source, cat# DMK27BUP031), and recording was started immediately without
423 acclimation. Images were captured through the IC Capture software (The Imaging
424 Source, version 2.5) under the following conditions: MJPEG Compressor for codec, a
425 frame rate of 0.87 fps, and an image size of Y800 (2592 × 1944). Locomotor activity
426 was quantified from the same video recordings used for larval sleep analysis. Travel
427 distance was calculated as the cumulative displacement of the larval centroid over time,
428 and locomotion speed was defined as total travel distance divided by the total duration
429 of wakefulness, considering only time bins classified as wake. To minimize the
430 possibility that feeding behavior was misclassified as sleep, we adjusted our immobility

threshold using video recordings in which larval feeding bouts, including relatively subtle episodes, were apparent, and configured the algorithm so that feeding-associated movements would generally be classified as wake rather than inactivity. During the development and routine use of the assay, we also inspected representative recordings across genotypes and did not observe obvious feeding-related abnormalities or gross locomotor defects under our HuginPC/IPC manipulations.

Sleep deprivation

Blue light irradiation was performed using a 455-nm LED (Thorlabs, cat# M455L4) with a collimating adapter (Thorlabs, cat# SM1U25-A) (Omamiuda-Ishikawa et al., 2020; Yoshino et al., 2017; Yoshino et al., 2025). The irradiation intensity was set to the maximum scale using a T-cube LED driver (Thorlabs, cat# LEDD1B). Temporal control of LED illumination was achieved using the Arduino UNO microcontroller board (Arduino, RRID:SCR_017284). For sleep deprivation experiments, the first 1 h was recorded without LED illumination, followed by another 1 h consisting of repeated cycles of "LED ON for 90 s and OFF for 30 s".

Immunohistochemistry

Antibody staining of larval neurons was carried out as previously reported (Morikawa et al., 2011; Omamiuda-Ishikawa et al., 2020). Briefly, dissection in phosphate-buffered saline (PBS); fixation in 4% paraformaldehyde/PBS at room temperature for either 90 min in CRTC::GFP experiments or 30 min in the others; washing with 0.3% Triton X-100/PBS (hereafter referred to as PBST) for 10 min × 3; blocking in 5% normal goat serum (NGS)/PBST at room temperature for 30 min; primary antibody treatment at 4°C overnight; washing with PBST for 10 min × 3; secondary antibody treatment at 4°C overnight; washing with PBST for 10 min × 3; and mounting in VECTASHIELD medium (Vector Laboratories, cat# H-1000, RRID:AB_2336789). Reactions were performed either in Terasaki 96-well plates (stem Corp., cat# P96R37N) for adults or in 48-well culture plates (Corning, cat# 3548) for larvae. The following primary antibodies were diluted in 5% NGS/PBST: chicken polyclonal anti-GFP (1:1000, Aves Labs, cat# GFP-1020, RRID:AB_10000240), mouse monoclonal anti-mCherry (1:1000, Takara Bio, cat# 632543, RRID:AB_2307319), rabbit polyclonal anti-Dilp3 (1:250, (Veenstra

463 et al., 2008)), rabbit polyclonal anti-Dilp2 (1:2000, (Okamoto et al., 2012)), mouse
464 monoclonal anti-BRP (1:100, Developmental Studies Hybridoma Bank, clone nc82;
465 RRID:AB_2314866), and rat monoclonal anti-histone H3 phospho S28 (1:1000,
466 Abcam, cat# ab10543; RRID:AB_2295065). The following secondary antibodies were
467 diluted in 5% NGS/PBST: goat anti-chicken Alexa Fluor 488 (1:200, Thermo Fisher
468 Scientific, cat# A-11039, RRID:AB_2534096), goat anti-mouse Alexa Fluor 555
469 (1:200, Thermo Fisher Scientific, cat# A-21424, RRID:AB_141780), goat anti-rabbit
470 Alexa Fluor 633 (1:200, Thermo Fisher Scientific, cat# A-21071, RRID:AB_2535732),
471 and goat anti-rat Alexa Fluor 633 (1:200, Thermo Fisher Scientific, cat# A-21094;
472 RRID:AB_2535749). Fluorescence images were obtained using a confocal microscope
473 (Leica, TCS SP8) with 20× (Leica, HC PL APO CS2 20×/0.75 IMM) and 63× (Leica,
474 HC PL APO CS2 63×/1.40 OIL) objectives. Images were captured at 512 × 512-pixel
475 resolution with an interval of 1 μm. Z-stack images of the maximum projections were
476 generated using the ImageJ v1.53t software (Schneider et al., 2012);
477 RRID:SCR_003070).
478
479 **Generation of transgenic lines**
480 *HugPC-LexA* lines were generated by ΦC31 integrase-mediated transgenesis, as
481 previously described (Groth et al., n.d.).
482 The 544-bp enhancer region of *Hug*, essentially the same as that used to generate
483 *HugPC-GAL4* (Hückesfeld et al., 2016), was PCR-amplified from fly genomic DNA.
484 The gel-purified amplicon was subjected to another round of PCR to add hangout
485 sequences. The backbone suicide-vector pBPnlsLexA::p65Uw (RRID:Addgene_26230)
486 was initially amplified by transforming the *ccdB*-resistant *E. coli* strain, One Shot™
487 *ccdB* Survival™ 2 $T1^R$ competent cells (Thermo Fisher Scientific, cat# A10460). The
488 PCR product and the vector were double-digested by Aat II (NEB, cat# R0117S) and
489 Fse I (NEB, cat# R0588S), followed by ligation using In-Fusion HD Cloning Kit
490 w/Cloning Enhancer (Takara Bio, cat# 639635). The integrity of the resulting plasmid
491 was confirmed by DNA sequencing. Plasmid insertion was targeted to four attP sites
492 (attP2, attP40, VK00005, and su(Hw)attP5) individually through ΦC31 integrase-
493 mediated transgenesis by BestGene Inc. (Chino Hills, CA). Transformants were selected
494 based on the eye color marker. Among the generated strains harboring *HugPC-LexA* in

495 each insertion site, labeling patterns in the larval brain were checked by driving
496 fluorescent marker expression under the control of *LexAop* (Figure 3—figure
497 supplement 2). As the *HugPC-LexA* inserted in attP2 closely resembled the labeling
498 pattern of the original *HugPC-GAL4*, it was used in further experiments.
499 The following primers were used for cloning:
500 Forward primer for the *HugPC* enhancer; 1st round PCR against genomic DNA:
501 5'-AAGGGTTTGGTTTAATTTATTTATGTCATA-3'
502 Reverse primer for the *HugPC* enhancer; 1st round PCR against the genomic DNA:
503 5'-GGACAACTGATGCCAGCAGC-3'
504 Forward primer for the *HugPC* enhancer with hangout sequences (underlined); 2nd
505 round PCR against the 1st round amplicon:
506 5'-gaaaagtgccacctgacgtAAGGGTTTGGTTTAATTTATTTATGTCATA-3'
507 Reverse primer for the *HugPC* enhancer with hangout sequences (underlined); 2nd round
508 PCR against the 1st round amplicon:
509 5'-cccgggcgagctcggccggGGACAACTGATGCCAGCAGC-3'
510
511
512 **Food intake assay**
513 Food intake was measured using a dye-based feeding assay adapted from Hückesfeld et
514 al. (2016). Apple juice agar plates were prepared with a spot of red yeast paste in the
515 center. After 30 min starvation, larvae were transferred onto the yeast paste and
516 videotaped for 20 min. Larvae were then collected in a small cell strainer and rinsed
517 with 60°C hot water to remove external dye, transferred to glass slides, and
518 photographed. Images were analyzed in ImageJ by measuring the area of red-stained
519 dye signal and the total body area, and food intake was quantified as the ratio of dye-
520 stained area to total body area for each larva.
521
522 **Measurement of neuronal activity and Dilp3 accumulation in IPCs**
523 The GFP-tagged CRTC (CRTC::GFP) reporter was applied to quantify the activities of
524 larval IPCs, essentially according to the previous report in adult flies (Bonheur et al.,
525 2023).
526 Parental *Dilp3-GAL4* and the reporter line harboring *UAS-CRTC::GFP* and *UAS-*

527 *mCD8::mCherry* (BDSC# 99657) were crossed, and eggs were collected within an 8–10
528 h time window. Offspring larvae were reared for 4 d after egg laying (AEL) at 25°C to
529 early third instar. Collected larvae were washed with water and starved on water-soaked
530 paper for 12–14 h. For *in vivo* thermogenetic activation, larva-containing Petri dishes
531 were warmed at 30°C for 60 min. For *ex vivo* thermogenetic experiments, larvae were
532 dissected in calcium- and sugar-free HL3.1 buffer (Nakamizo-Dojo et al., 2023)) at
533 30°C, and each brain was incubated in the same buffer at 30°C for 5 min. For *ex vivo*
534 glucose or peptide application assays, larvae were first dissected in the same buffer as
535 above at room temperature, and brain samples were then treated with either 20 mM D-
536 glucose or 1 mM of chemically synthesized peptides dissolved in HL3.1 buffer for 5
537 min. After incubation, samples were subjected to immunohistochemical analyses to
538 visualize GFP, mCherry, and Dilp3 signals (see the section "Immunohistochemistry").
539 Image processing was performed using ImageJ v1.53t ((Schneider et al., 2012);
540 RRID:SCR_003070). Nuclear ROIs and cell body outlines were drawn based on the
541 mCD8::mCherry fluorescence insensitive to neuronal activity, and the mean intensities
542 of CRTC::GFP signals within the nucleus (F_{nuc}) and the cytoplasm ($F_{cyto} = F_{whole\ cell} -$
543 F_{nuc}) were quantified. NLI was calculated using the following formula: ($F_{nuc} -$
544 F_{cyto})/($F_{nuc} + F_{cyto}$). To assess Dilp3 accumulation in IPCs, the anti-Dilp3 signal intensity
545 was measured within the cytosol of each cell, excluding the nucleus. Data from 4-14
546 Dilp3-positive IPCs per brain, collected from 3-7 larvae, were pooled for each
547 genotype/treatment group.
548 We attempted to record GCaMP-based calcium dynamics in Hugin neurons and IPCs,
549 but did not pursue this approach further because it was low-throughput and a positive-
550 control assay (glucose application) did not elicit the expected IPC calcium response in
551 our hands.
552
553 **Chemical synthesis of Hug peptides**
554 Peptides with the following amino acid sequences were chemically synthesized using
555 the Fmoc solid phase method, and their purity was assessed by HPLC to be over 95%.
556 All procedures were carried out by Eurofins Genomics K.K. (Tokyo, Japan).
557 *Drosophila* Hug-γ:
558 Acetyl-QLQSNGEPAYRVRTPRL-CONH2 (17 a.a.)

559 *Drosophila* PK-2:
560 Acetyl-SVPFKPRL-CONH2 (8 a.a.)
561 Human NMU:
562 Acetyl-FRVDEEFQSPFASQSRGYFLFRPRN-CONH2 (25 a.a.)
563
564 **Sleep quantification in adult flies**
565 The following parts of the *Drosophila* activity monitor (DAM) system were purchased
566 from TriKinetics Inc. (Waltham, MA): the *Drosophila* Activity Monitor (cat# DAM2),
567 the power supply interface unit (cat# PSIU9), monitor tubes with an outside diameter of
568 5 mm and a length of 65 mm (cat# PGT5x65), and tube caps (cat# CAP5-Black). Newly
569 eclosed adult flies were collected under brief CO_2 anesthesia and kept as groups of 10–
570 15 in standard food vials. Males and females were kept separately to avoid mating. To
571 minimize disturbance by noise and vibration, flies were placed inside a fan-less Peltier-
572 type incubator (Mitsubishi Electric Engineering Co., Ltd., cat# SLC-25) set to 25°C,
573 externally connected with 5-mm diameter LED lights (MY-CRAFT, Ltd., cat#
574 5W0601) and a timer device (Panasonic Corp., cat# WH3311WP) to generate a
575 9AM:9PM light/dark cycle. After 3 d of eclosion, each fly was gently aspirated into a
576 Pyrex glass monitor tube, one end of which was stuffed with agar food (2% (w/w) agar,
577 5% (w/w) sucrose), and the other was plugged with a cotton string. The tubes were set
578 to the monitor device and placed inside the same fan-less incubator. The DAM system
579 was connected to an external PC installed with DAMSystem3 Data Collection Software
580 (RRID:SCR_021809; available at https://trikinetics.com/) for data acquisition, and
581 beam-crossing by each fly was counted for two successive days. Time windows longer
582 than 5 min without beam-crossing were judged as sleep bouts, following the
583 conventional criteria for adult fly sleep (Paul J. Shaw, Chiara Cirelli, Ralph J.
584 Greenspan, & Giulio Tononi, 2000).
585
586 **Statistical analysis**
587 Statistical analyses by Kruskal–Wallis one-way ANOVA, Mann–Whitney U-test, or
588 chi-square test were performed using Prism 9.5.1 (GraphPad, RRID:SCR_002798).
589 Bonferroni correction was applied for multiple comparisons. Asterisks (*) represent p-
590 values as indicated within each figure legend. All data necessary to reproduce the figure

panels and statistical analyses are available as Source Data files.

Acknowledgements

We thank Y. Rao, M. Pankratz, S. Waddel, and the Bloomington *Drosophila* Stock Center for fly stocks; J. A. Veenstra for the anti-Dilp3 antibody; T. Nishimura for the anti-Dilp2 antibody; Y. Nishizuka for valuable suggestions on writing code for automated larval detection and sleep quantification; H. Ito, N. Yamaji, M. Maetani, A. Ogasawara, E. Kato, T. Rikiishi, S. Ando, M. Hayashi, and S. Miyazaki for technical assistance and fly maintenance; and the members of Emoto Lab for critical comments and discussion. This work is supported by MEXT Grants-in-Aid for Scientific Research on Innovative Areas "Dynamic regulation of brain function by Scrap and Build system" (KAKENHI 16H06456), JSPS (KAKENHI 16H02504), WPI-IRCN, AMED-CREST (JP22gm310010), JSTCREST, Toray Foundation, Naito Foundation, Takeda Science Foundation, and Uehara Memorial Foundation to K.E.; the Leading Initiative for Excellent Young Researchers (LEADER) from MEXT, JSPS (KAKENHI 22K06309), and AMED-PRIME (JP22gm6510011) to K.I.; Grant-in-Aid for JSPS Fellows (24KJ0911) to M.M.; and Grant-in-Aid for JSPS Fellows (22J21096; 22KJ1042) to C.H.

610 **Figures and Legends**

611 **Figure 1. PK2-R1 is required for larval sleep control**

612 (A) Sleep amounts in *PK2-R1* or *Oamb* knockout mutants. Each dot represents an
613 individual animal; in this and the following panels, "N" indicates the number of
614 biologically independent animals per group, and the thick line and thin error bars
615 indicate the median and interquartile range (Q1–Q3), respectively. *** $p < 0.001$
616 (Mann–Whitney U-test with Bonferroni correction). (B) Sleep amounts in larvae in
617 which *PK2-R1* neurons were silenced. *** $p < 0.001$ (Mann–Whitney U-test with
618 Bonferroni correction). (C) Expression pattern of *PK2-R1-GAL4 > UAS-Kir::EGFP*
619 larvae.

620

621 **Figure 1—figure supplement 1. Detailed experimental setup for analyzing larval**
622 **sleep**

623 (A) Schematic flow of automated larval sleep quantification. A second instar larva was
624 placed in each of 24 wells, and all 24 wells were videotaped from above. For each well
625 and frame, the image of larva was blurred and binarized to automatically locate the
626 larva. Consecutive frames were then compared so that changes in pixel values were
627 summed to estimate larval motion. This motion estimate was then used to classify every
628 consecutive pair of frames as representing "active" or "inactive." We found that
629 inactivity across 12 consecutive frames meets the sleep criteria, as shown in Figure 1—
630 figure supplement 2. (B) Schematic representation of the 24-well chamber used for
631 larval sleep assays. (C) Flow of automated processes of larval motion detection and
632 active/inactive state determination. For each well and frame, the image of larva was
633 blurred and binarized. Consecutive frames were then compared so that changes in pixel
634 values were summed to estimate larval motion. This motion estimate was then used to
635 classify every consecutive pair of frames as representing "active" or "inactive."

636

637 **Figure 1—figure supplement 2. Larval "sleep state" in this study is consistent with**
638 **behavioral criteria for sleep**

639 (A) Relationship between "inactive" state duration and spontaneous arousal probability.
640 Sustained quiescence for ≥ 12 frames (open circles) significantly reduced arousal
641 probability compared to 1-frame inactivity. * $p < 0.05$, NS: $p \geq 0.05$ (chi-squared test).
642 (B) The percentage of larvae that showed a response within the next 10 frames after
643 high-intensity blue light. The number of events analyzed was 36 and 60 with and
644 without blue light irradiation, respectively. * $p < 0.05$ (Fisher's exact test). (C) Sleep
645 amounts before, during, and after blue light irradiation. The number of larvae tested was
646 21 and 21 for the control and experimental groups, respectively. ** $p < 0.01$, NS: $p \geq$
647 0.05 (Mann–Whitney U-test with Bonferroni correction). (D) Percentage of larvae that
648 showed a response in the next 1 or 12 frames after blue light stimulation. Number of
649 events analyzed: 1960 or 111 for 1- or 12-frame continuous inactivity prior to blue light
650 illumination, respectively. **** $p < 0.0001$ (chi-squared test).

651

652

653 **Figure 1—figure supplement 3. CRISPR-knock-out screen for genes that regulate**
654 **larval sleep.**

655 Total sleep amounts in CRISPR-knock-out mutants were measured for 18 h from the
656 beginning of the second instar. The data for Control, *PK2-R1,* and *Oamb* mutants are
657 identical to those shown in Figure 1. Box plots are generated so that the center line
658 indicates the median, the box limits indicate the upper and lower quartiles, and the
659 whiskers indicate the minimum-to-maximum range. *** $p < 0.005$ (Kruskal–Wallis
660 one-way ANOVA and post hoc Mann–Whitney U-test with Bonferroni correction).
661 Number of larvae tested: 475 for the control and 10–52 for each mutant.

662

663

664 **Figure 1—figure supplement 4. Effects of neuronal manipulation on larval sleep**

665 Sleep amounts in larvae in which distinct neuronal populations were silenced. Kir2.1
666 expression was driven by each enhancer-GAL4 for "hit" genes identified in the
667 CRISPR-knock-out screen. Each dot represents an individual animal in these panels,
668 "N" indicates the number of biologically independent animals per group, and the thick
669 line and thin error bars indicate the median and interquartile range (Q1–Q3),
670 respectively. *** $p < 0.001$, ** $p < 0.01$, * $p < 0.05$, NS: ≥ 0.05 (Mann–Whitney U-test
671 with Bonferroni correction)

672

673 **Figure 1—figure supplement 5. Larval sleep phenotypes in PK2-R1 mutants**
674 **quantified over 18 h and the first 6 h.**

675 (A–C) Sleep metrics quantified over an 18-hour period in second-instar larvae, whereas
676 (D–F) show the same metrics quantified over the first 6 hours in the same animals.
677 Total sleep is shown in (A) and (D), bout number in (B) and (E), and mean bout length
678 in (C) and (F). Each dot represents an individual larva; the thick line indicates the
679 median and the thin error bars indicate the interquartile range (Q1–Q3). Numbers in
680 parentheses indicate N, the number of biologically independent animals per group. ** p
681 < 0.01, * $p < 0.05$, NS: ≥ 0.05 (Mann–Whitney U-test with Bonferroni correction).

682

683

684 **Figure 2. IPCs and Dilps negatively regulate larval sleep**

685 (A) Triple labeling of *PK2-R1* neurons expressing nuclear-localized RFP (magenta),
686 *Dilp3* neurons expressing nuclear-localized GFP (green), and anti-Dilp2 positive cells
687 (blue). Top panels show signals in the larval brain and the VNC. Bottom panels show
688 magnified images of the white-squared area in each top panel, focusing on the
689 dorsomedial brain region where the cell bodies of IPCs are located. Note that all IPCs
690 labeled with *Dilp3-GAL4* overlapped with $PK2\text{-}R1^{2A\text{-}LexA}$-expressing cells. Similar
691 results were obtained from 5 independent samples of the same genotype. (B)
692 Simultaneous detection of *PK2-R1* neurons expressing nuclear-localized RFP
693 (magenta), *Dilp5* neurons expressing nuclear-localized GFP (green), and anti-Dilp2

694 positive cells (blue). Similar results were obtained from 5 independent samples of the
695 same genotype. (C) Effect of IPCs silencing on larval sleep. Each dot represents an
696 individual animal; in this and the following panels, “N” indicates the number of
697 biologically independent animals per group, and the thick line and thin error bars
698 indicate the median and interquartile range (Q1–Q3), respectively. *** $p < 0.001$, ** p
699 < 0.01, * $p < 0.05$ (Mann–Whitney U-test with Bonferroni correction). (D) Sleep
700 amounts in *Dilp3* or *Dilp5* null mutants. *** $p < 0.001$, ** $p < 0.01$ (Mann–Whitney U-
701 test with Bonferroni correction).
702

703 **Figure 2—figure supplement 1. Locomotion speeds are not consistently affected by**
704 **genetical manipulations of *PK2-R1*, IPCs, or *Dilps***
705 (A) Larval locomotion speed in controls and PK2-R1 mutants. (B-C) Effects of
706 silencing PK2-R1 neurons (B) and IPCs (C) on larval locomotion speed, shown together
707 with the corresponding genetic controls. (D) Larval locomotion speed in Dilp3 or Dilp5
708 null mutants. Average locomotion speed during wake periods was calculated from the
709 datasets shown in Figures 1A, 1B, 2C, and 2D. N indicates the number of biologically
710 independent larvae per group. Each dot represents an individual larva; thick lines
711 indicate the median and thin error bars indicate the interquartile range (Q1-Q3). *** $p <$
712 0.0001, * $p < 0.05$, NS: $p \geq 0.05$ (Mann-Whitney U-test with Bonferroni correction).
713
714

715 **Figure 3. *Hug* neurons negatively regulate larval sleep**

716 (A) Sleep amounts in *Hug* CRISPR-knockout mutant larvae. **** $p < 0.0001$ (Mann–
717 Whitney U-test). Each dot represents an individual animal; in this and the following
718 panels, "N" indicates the number of biologically independent animals per group, and the
719 thick line and thin error bars indicate the median and interquartile range (Q1–Q3),
720 respectively. (B) Effect of silencing Hug neurons on larval sleep amount. ** $p < 0.01$, *
721 $p < 0.05$ (Mann–Whitney U-test with Bonferroni correction). (C) Larval sleep changes
722 induced by optogenetic activation of *Hug* neurons. For each genotype, sleep duration in
723 the 1-h light-ON period was normalized to that in the 1-h light-OFF phase. * $p < 0.05$
724 (Mann–Whitney U-test with Bonferroni correction). (D) Larval sleep during
725 thermogenetic activation of *Hug* neurons. ** $p < 0.01$, * $p < 0.05$ (Mann–Whitney U-
726 test with Bonferroni correction). (E) Visualization of HugPC neurons and IPCs labeled
727 by rCD2::RFP (magenta) and mCD8::GFP (green), respectively. The bottom panels
728 show magnified images of the white-squared dorsomedial region in the top panels,
729 where HugPC neurons project their axons close to the cell bodies of the IPCs. While the
730 top panels are z-stacks of 122 image slices (1 μm interval) covering the entire brain
731 tissue, the bottom panels are projections of 60 slices centering around IPCs. Similar
732 results were obtained from 5 independent samples of the same genotype. (F) The effect
733 of neuronal silencing confined to the HugPC subpopulation. ** $p < 0.01$, * $p < 0.05$

734 (Mann–Whitney U-test with Bonferroni correction).
735
736 **Figure 3—figure supplement 1. Effects of Hug pathway manipulations on larval**
737 **locomotion speed.**
738 (A) Locomotion speed of Hug knockout mutants during wake periods. (B) Effects of
739 silencing Hug neurons on locomotion speed. (C-D) Effects of activating Hug neurons
740 on locomotion speed, shown as the light ON/light OFF ratio (C) and the absolute
741 locomotion speed (D). (E) Effects of silencing HugPC neurons on locomotion speed.
742 Locomotion speed was quantified from the same videos used for the larval sleep assays
743 in Figure 3. Each dot represents an individual larva; thick lines indicate the median and
744 thin error bars indicate the interquartile range (Q1-Q3). N indicates the number of
745 biologically independent animals per group. NS $p \geq 0.05$ (Mann-Whitney U-test) in (A).
746 *** $p < 0.0001$, * $p < 0.05$, NS $p \geq 0.05$ (Mann-Whitney U-test with Bonferroni
747 correction) in (B-E).
748
749 **Figure 3—figure supplement 2. Generation of *HugPC-LexA* transgenic lines**
750 (A-D) Labeling patterns of four *HugPC-LexA* strains in larval CNS visualized by
751 rCD2::RFP. Four transgenic lines were generated by injecting the same plasmid into the
752 following landing sites individually: su(Hw)attP5, VK00005, attP2, and attP40.
753 Magenta arrowheads represent cell bodies apparently located outside the previously
754 classified HugPC subpopulation (Bader et al., 2007).
755
756 **Figure 3—figure supplement 3. Silencing HugPC neurons reduces larval food**
757 **intake measured by a dye-based assay.**
758 After a 30 min starvation, larvae were allowed to feed on red yeast paste placed on an
759 apple juice agar plate, and food intake was quantified as the ratio of the red dye-stained
760 body surface area to the total body surface area (ImageJ). Each dot represents an
761 individual larva; the thick line indicates the median and the thin error bars indicate the
762 interquartile range (Q1–Q3). ** $p < 0.01$ (Mann–Whitney U-test).
763
764 **Figure 4. Activation of Hug neurons triggers Ca2+ responses in larval IPCs.**

765 (A) Schematic workflow for assessing intracellular Ca2+ levels in IPCs while
766 thermogenetically activating Hug neurons. Larvae were exposed to low (18°C) or high
767 (30°C) temperature for 1 h, followed by imaging of CRTC::GFP in IPCs and calculation
768 of the CRTC::GFP nuclear localization index (NLI; see Methods). (B–C) Nuclear-
769 localized CRTC::GFP signal (CRTC::GFP NLI) in larval IPCs under low-temperature
770 (B) or high-temperature (C) conditions, with or without thermogenetic activation of
771 Hug neurons. Each dot represents an individual cell; the thick line indicates the median
772 and the thin error bars indicate the interquartile range (Q1–Q3). "N" indicates the
773 number of cells analyzed per group. **** $p < 0.0001$, NS $p \geq 0.05$ (Mann–Whitney U-
774 test). (D) Working model of a neuronal network in which Hug neurons activate IPCs to
775 regulate larval sleep
776
777 **Figure 4-figure supplement 1. Axonal projections of HuginPC neurons visualized**
778 **with a presynaptic marker.**
779 Representative whole-mount image of the larval central nervous system showing Syt-
780 eGFP signals expressed in HuginPC neurons. Scale bar, 100 µm.
781
782 **Figure 5. Hug peptides induce Ca^{2+} responses in larval IPCs via PK2-R1**
783 (A) Schematic flow of peptide application followed by Ca^{2+} imaging. (B–C) Ca^{2+}
784 responses in laval IPCs during *ex vivo* bath application of either glucose (B) or Hug
785 peptides (C). In this and the following panels, 'N' indicates the number of cells used for
786 each group, and the thick line and thin error bar represent the median and interquartile
787 range (Q1–Q3), respectively. **** $p < 0.0001$, *** $p < 0.001$ (Mann–Whitney U-test
788 with Bonferroni correction). (D) Representative images of larval IPCs upon peptide
789 application. Scale bars, 2 µm. (E) Anti-Dilp3 signal intensity measured within the
790 cytosolic areas of larval IPCs. *** $p < 0.001$, * $p < 0.05$ (Mann–Whitney U-test with
791 Bonferroni correction). (F–G) Ca^{2+} responses in larval IPCs derived from *PK2-R1*
792 knockout mutants, measured after either glucose (F) or Hug peptide application (G). **
793 $p < 0.01$, NS $p \geq 0.05$ (Mann–Whitney U-test with Bonferroni correction). (H) A model
794 where Hug peptides, but not glucose, activate IPCs via the PK2-R1 receptor in the
795 larval brain.

796

797 **Figure 5—figure supplement 1. D-glucose but not Hug peptide cause Dilp2**
798 **reduction in larval IPCs**

799 (A–B) Anti-Dilp2 signal intensity measured in larval IPCs after glucose (A) or Hug-γ
800 application (B). In this and the following panels, 'N' indicates the number of cells used
801 for each group, and the thick line and thin error bar represent the median and
802 interquartile range (Q1–Q3), respectively. **** $p < 0.0001$, * $p < 0.05$ (Mann–Whitney
803 U-test). (C) Anti-Dilp3 signal intensity measured within the cytosolic areas of larval
804 IPCs. NS ≥ 0.05 (Mann–Whitney U-test).
805

806 **Figure 5—figure supplement 2. Representative images of Dilp3 immunoreactivity**
807 **in larval IPCs after bath application of Hug-γ peptide.**
808 Larval IPCs were labeled with Dilp3>mCherry (top row), and endogenous Dilp3 was
809 detected by anti-Dilp3 immunostaining (bottom row). Representative brains from
810 buffer-only controls (Brain #1 and #2) and Hug-γ peptide application (Brain #3 and #4)
811 are shown. Scale bars: 25 μm (Brains #1–3) and 10 μm (Brain #4).
812

813 **Figure 6. Distinct impacts of Hugin/PK2-R1 axis on wake/sleep control in larvae**
814 **and adult**

815 (A) Total sleep amounts in *Hug kno*ckout mutant adults. NS $p \geq 0.05$ (Mann–Whitney
816 U-test). In these and the following panels, 'N' indicates the number of biologically
817 independent animals used for each group, and the thick line and thin error bar represent
818 the median and interquartile range (Q1–Q3), respectively. NS $p \geq 0.05$ (Mann–Whitney
819 U-test). (B) Sleep amounts of adults in which HugPC neurons were silenced. *** $p <$
820 0.001, NS $p \geq 0.05$ (Mann–Whitney U-test with Bonferroni correction). (C) Sleep
821 amounts of *Dilp3* or *Dilp5* null mutant adults. *** $p < 0.001$ (Mann–Whitney U-test
822 with Bonferroni correction). (D) Schematic flow of peptide application experiments
823 using adult brains. (E–F) Ca^{2+} sponses (E) or anti-Dilp3 signal intensity (F) in adult
824 IPCs after Hug peptide application. ** $p < 0.01$, NS $p \geq 0.05$ (Mann–Whitney U-test
825 with Bonferroni correction).

826
827
828 **Figure 6—figure supplement 1. Sleep patterns of adult flies with genetical**
829 **manipulations in the Hugin and insulin pathways**

830 (A) Experimental setup for monitoring adult sleep using the *Drosophila* Activity
831 Monitor (DAM). (B) Total daily sleep duration in adult flies carrying CRISPR-
832 knockout mutations in genes whose larval sleep was significantly altered in Figure 1B.
833 Each dot represents an individual fly; the thick line indicates the median and the thin
834 error bars indicate the interquartile range (Q1–Q3). *** $p < 0.01$, ** $p < 0.05$ (Kruskal–
835 Wallis one-way ANOVA followed by post hoc Mann–Whitney U-test with Bonferroni
836 correction). (C) Daytime (left) and nighttime (right) sleep amounts in flies in which
837 HugPC neurons were silenced. (D) Daytime (left) and nighttime (right) sleep amounts
838 in Dilp3 or Dilp5 null mutants. In (C) and (D), numbers in parentheses indicate N, the
839 number of biologically independent animals per group. *** $p < 0.001$, ** $p < 0.01$, * p
840 < 0.05, NS $p \geq 0.05$ (Mann–Whitney U-test with Bonferroni correction).
841
842 **Figure 6—figure supplement 2. Morphologies of *PK2-R1* neurons, HugPC neurons,**
843 **and IPCs in the adult brain.**
844 (A) Dual labeling of *PK2-R1* neurons and IPCs expressing nuclear-localized RFP
845 (magenta) and GFP (green), respectively. The top panels show signals in the entire adult
846 brain. The bottom panels show magnified images of the white-squared area in each
847 corresponding top panel, focusing on the dorsomedial brain region where the cell bodies
848 of IPCs are located. Similar results were obtained from 5 independent samples of the
849 same genotype. (B) Visualization of HugPC neurons and IPCs labeled by mCD8::GFP
850 (magenta) and the anti-Dilp3 antibody (green), respectively. Similar results were
851 obtained from 4 independent samples of the same genotype.
852
853
854 **Figure 6—figure supplement 3. Adult sleep architecture and waking activity**
855 **following genetic manipulations of the hugin and insulin pathways.**
856 (A) Bout number per day (left), mean bout length (middle), and mean beam crossings

during wakefulness (right) in Hug^attP mutants. (B) The same metrics in flies with HugPC neuron silencing. (C) The same metrics in Dilp3[1] and Dilp5^1 null mutants. (D) Total daily sleep in flies with Dilp3-positive neuron silencing. Each dot represents an individual fly; the thick line indicates the median and the thin error bars indicate the interquartile range (Q1–Q3). Numbers in parentheses indicate N, the number of biologically independent animals per group. * $p < 0.05$, ** $p < 0.01$, *** $p < 0.001$, NS $p \geq 0.05$ (Mann–Whitney U-test with Bonferroni correction).

Figure 7. A schematic model of the Hugin/PK2-R1/Dilps axis in larval and adult sleep

Schematic summary comparing larvae and adults. In larvae, bath application of hugin peptides activates IPCs, and both hugin signaling (HugPC neurons/hugin peptides) and IPC output (including Dilp3) act to suppress larval sleep. In adults, hugin peptides do not activate IPCs (dashed arrow), whereas IPC/Dilp3 signaling promotes adult sleep.

References

Ahnaou, A., & Drinkenburg, W. H. I. M. (2011). Neuromedin U2 receptor signaling mediates alteration of sleep-wake architecture in rats. *Neuropeptides*, 45(2), 165–174. Retrieved from https://doi.org/10.1016/j.npep.2011.01.004

Bader, R., Colomb, J., Pankratz, B., Schröck, A., Stocker, R. F., & Pankratz, M. J. (2007). Genetic dissection of neural circuit anatomy underlying feeding behavior in Drosophila: Distinct classes of hugin-expressing neurons. *Journal of Comparative Neurology*, 502(5), 848–856. Retrieved from https://doi.org/10.1002/cne.21342

Baines, R. A., Uhler, J. P., Thompson, A., Sweeney, S. T., & Bate, M. (2001). *Altered Electrical Properties in Drosophila Neurons Developing without Synaptic Transmission*.

Barlow, I. L., & Rihel, J. (2017, June 1). Zebrafish sleep: from geneZZZ to neuronZZZ. *Current Opinion in Neurobiology*. Elsevier Ltd. Retrieved from https://doi.org/10.1016/j.conb.2017.02.009

Blumberg, M. S., H Seelke, A. M., Lowen, S. B., & Karlsson, K. A. (2005). Dynamics of sleep–wake cyclicity in developing rats. *PNAS*, 102(41). Retrieved from www.pnas.orgcgidoi10.1073pnas.0506340102

Bonheur, M., Swartz, K. J., Metcalf, M. G., Wen, X., Zhukovskaya, A., Mehta, A., … Hattori, D. (2023). A rapid and bidirectional reporter of neural activity reveals neural correlates of social behaviors in Drosophila. *Nature Neuroscience*, 26(7), 1295–1307. Retrieved from https://doi.org/10.1038/s41593-023-01357-w

Burke, C. J., Huetteroth, W., Owald, D., Perisse, E., Krashes, M. J., Das, G., … Waddell, S. (2012). Layered reward signalling through octopamine and dopamine in Drosophila. *Nature*, 492(7429), 433–437. Retrieved from https://doi.org/10.1038/nature11614

Chiu, C. N., Rihel, J., Lee, D. A., Singh, C., Mosser, E. A., Chen, S., … Prober, D. A. (2016). A Zebrafish Genetic Screen Identifies Neuromedin U as a Regulator of Sleep/Wake States. *Neuron*, 89(4), 842–856. Retrieved from https://doi.org/10.1016/j.neuron.2016.01.007

Churgin, M. A., Szuperak, M., Davis, K. C., Raizen, D. M., Fang-Yen, C., & Kayser, M. S. (2019). Quantitative imaging of sleep behavior in Caenorhabditis elegans

and larval Drosophila melanogaster. *Nature Protocols 2019 14:5*, 14(5), 1455–1488. Retrieved 25 December 2021 from https://doi.org/10.1038/s41596-019-0146-6

Davis, K. F., Parker, K. P., & Montgomery, G. L. (2004). *Sleep in infants and young children: Part one: normal sleep*. *Journal of Pediatric Health Care* (Vol. 18, pp. 65–71). Mosby. Retrieved 25 December 2021 from https://doi.org/10.1016/S0891-5245(03)00149-4

Deng, B., Li, Q., Liu, X., Cao, Y., Li, B., Qian, Y., … Rao, Y. (2019). Chemoconnectomics: Mapping Chemical Transmission in Drosophila. *Neuron*, 101(5), 876-893.e4. Retrieved from https://doi.org/10.1016/j.neuron.2019.01.045

Dubowy, C., & Sehgal, A. (2017). Circadian rhythms and sleep in Drosophila melanogaster. *Genetics*, 205(4), 1373–1397. Retrieved from https://doi.org/10.1534/genetics.115.185157

Enell, L. E., Kapan, N., Söderberg, J. A. E., Kahsai, L., & Nässe, D. R. (2010). Insulin signaling, lifespan and stress resistance are modulated by metabotropic GABA receptors on insulin producing cells in the brain of Drosophila. *PLoS ONE*, 5(12). Retrieved from https://doi.org/10.1371/journal.pone.0015780

Frank, M. G., Ruby, N. F., Heller, H. C., & Franken, P. (2017). Development of circadian sleep regulation in the rat: A longitudinal study under constant conditions. *Sleep*, 40(3). Retrieved from https://doi.org/10.1093/sleep/zsw077

Furusawa, K., Ishii, K., Tsuji, M., Tokumitsu, N., Hasegawa, E., & Emoto, K. (2023). Presynaptic UBE3A E3 ligase promotes synapse elimination by downregulation of BMP signaling. *Science*, 381, 1197-1205. Retrieved from http://doi.org/ 10.1126/science.ade8978.

Groth, A. C., Fish, M., Nusse, R., & Calos, M. P. (2004). Construction of Transgenic Drosophila by Using the Site-Specific Integrase From Phage φC31. *Genetics*, (166), 1775–1782. Retrieved from https://academic.oup.com/genetics/article/166/4/1775/6052665

Hamada, F. N., Rosenzweig, M., Kang, K., Pulver, S. R., Ghezzi, A., Jegla, T. J., & Garrity, P. A. (2008). An internal thermal sensor controlling temperature preference in Drosophila. *Nature*, 454(7201), 217–220. Retrieved from https://doi.org/10.1038/nature07001

941 Hendricks, J. C., Lu, S., Kume, K., Yin, J. C. P., Yang, Z., & Sehgal, A. (2003). Gender
942 dimorphism in the role of cycle (BMAL1) in rest, rest regulation, and longevity in
943 Drosophila melanogaster. *Journal of Biological Rhythms*, 18(1), 12–25. Retrieved
944 from https://doi.org/10.1177/0748730402239673
945 Hückesfeld, S., Peters, M., & Pankratz, M. J. (2016). Central relay of bitter taste to the
946 protocerebrum by peptidergic interneurons in the Drosophila brain. *Nature*
947 *Communications*, 7. Retrieved from https://doi.org/10.1038/ncomms12796
948 Hückesfeld, S., Schlegel, P., Miroschnikow, A., Schoofs, A., Zinke, I., Haubrich, A. N.,
949 … Pankratz, M. J. (2021). Unveiling the sensory and interneuronal pathways of
950 the neuroendocrine connectome in Drosophila. *ELife*. Retrieved from
951 https://doi.org/10.7554/eLife
952 Inagaki, H. K., Jung, Y., Hoopfer, E. D., Wong, A. M., Mishra, N., Lin, J. Y., …
953 Anderson, D. J. (2014). Optogenetic control of Drosophila using a red-shifted
954 channelrhodopsin reveals experience-dependent influences on courtship. *Nature*
955 *Methods*, 11(3), 325–332. Retrieved from https://doi.org/10.1038/nmeth.2765
956 Lakhotia SC, Ranganath HA, editors. 2021. *Experiments with Drosophila for Biology*
957 *Courses*. Indian Academy of Sciences, Bengaluru, India.
958 Kitatani, Y., Tezuka, A., Hasegawa, E., Yagagi, S., Togashi, K., Tsuji, M., Kondo, S.,
959 Parrish, J. Z., & Emoto, K. (2020). *Drosophila miR-87* promotes dendrite
960 regeneration by targeting the transcriptional repressor Tramtrack69. *PLoS*
961 *Genetics,* 16, e1008942.
962 Kréneisz, O., Chen, X., Fridell, Y. W. C., & Mulkey, D. K. (2010). Glucose increases
963 activity and Ca2+ in insulin-producing cells of adult Drosophila. *NeuroReport*,
964 21(17), 1116–1120. Retrieved from
965 https://doi.org/10.1097/WNR.0b013e3283409200
966 Kume, K., Kume, S., Park, S. K., Hirsh, J., & Jackson, F. R. (2005). Dopamine Is a
967 Regulator of Arousal in the Fruit Fly. *Journal of Neuroscience*, 25(32), 7377–
968 7384. Retrieved 10 December 2024 from
969 https://doi.org/10.1523/JNEUROSCI.2048-05.2005
970 Morikawa, R., Kanamori, T., Yasunaga, K., & Emoto, K. (2011). Different levels of the
971 TRIM protein Asap regulate distinct axonal projections of *Drosophila* sensory
972 neurons. *Proceedings of the National Academy of Sciences of the United States of*

America, 108, 19389-19394.

Nakamizo-Dojo, M., Ishii, K., Yoshino, J., Tsuji, M., & Emoto, K. (2023). Descending GABAergic pathway links brain sugar-sensing to peripheral nociceptive gating in Drosophila. *Nature Communications*, 14(1). Retrieved from https://doi.org/10.1038/s41467-023-42202-9

Oh, Y., Lai, J. S. Y., Mills, H. J., Erdjument-Bromage, H., Giammarinaro, B., Saadipour, K., … Suh, G. S. B. (2019). A glucose-sensing neuron pair regulates insulin and glucagon in Drosophila. *Nature*, 574(7779), 559–564. Retrieved from https://doi.org/10.1038/s41586-019-1675-4

Ohhara, Y., Blick, M., Park, D., Yoon, S. E., Kim, Y. J., Pankratz, M. J., … Yamanaka, N. (2024). A Neuropeptide Signaling Network That Regulates Developmental Timing and Systemic Growth in Drosophila. *The Journal of Comparative Neurology*, 532(10), e25677. Retrieved from https://doi.org/10.1002/cne.25677

Okamoto, N., Nishimori, Y., & Nishimura, T. (2012). Conserved role for the Dachshund protein with Drosophila Pax6 homolog eyeless in insulin expression. *Proceedings of the National Academy of Sciences of the United States of America*, 109(7), 2406–2411. Retrieved from https://doi.org/10.1073/pnas.1116050109

Omamiuda-Ishikawa, N., Sakai, M., & Emoto, K. (2020). A pair of ascending neurons in the subesophageal zone mediates aversive sensory inputs-evoked backward locomotion in *Drosophila* larvae. *PLoS Genetics,* 16, e1009120.

Paul J. Shaw, Chiara Cirelli, Ralph J. Greenspan, & Giulio Tononi. (2000). Correlates of Sleep and Waking in Drosophila melanogaster. *SCIENCE*, (287), 1834–1837.

Poe, A. R., Zhu, L., Szuperak, M., Mcclanahan, P. D., Anafi, R. C., Scholl, B., … Kayser, M. S. (2023). *Developmental emergence of sleep rhythms enables long-term memory in Drosophila*. Retrieved from https://www.science.org

Raizen, D. M., Zimmerman, J. E., Maycock, M. H., Ta, U. D., You, Y. J., Sundaram, M. V., & Pack, A. I. (2008). Lethargus is a Caenorhabditis elegans sleep-like state. *Nature*, 451(7178), 569–572. Retrieved from https://doi.org/10.1038/nature06535

Rosenkilde, C., Cazzamali, G., Williamson, M., Hauser, F., Søndergaard, L., DeLotto, R., & Grimmelikhuijzen, C. J. P. (2003). Molecular cloning, functional expression, and gene silencing of two Drosophila receptors for the Drosophila

1005 neuropeptide pyrokinin-2. *Biochemical and Biophysical Research*
1006 *Communications*, 309(2), 485–494. Retrieved from
1007 https://doi.org/10.1016/j.bbrc.2003.08.022
1008 Scammell, T. E., Arrigoni, E., & Lipton, J. O. (2017, February 22). 【Review】Neural
1009 Circuitry of Wakefulness and Sleep. *Neuron*. Cell Press. Retrieved from
1010 https://doi.org/10.1016/j.neuron.2017.01.014
1011 Schlegel, P., Texada, M. J., Miroschnikow, A., Schoofs, A., Hückesfeld, S., Peters, M.,
1012 … Pankratz, M. J. (2016a). Synaptic transmission parallels neuromodulation in a
1013 central food-intake circuit. *ELife*, 5(NOVEMBER2016). Retrieved from
1014 https://doi.org/10.7554/eLife.16799.001
1015 Schlegel, P., Texada, M. J., Miroschnikow, A., Schoofs, A., Hückesfeld, S., Peters, M.,
1016 … Pankratz, M. J. (2016b). Synaptic transmission parallels neuromodulation in a
1017 central food-intake circuit. *ELife*, 5(NOVEMBER2016). Retrieved from
1018 https://doi.org/10.7554/eLife.16799.001
1019 Schneider, C. A., Rasband, W. S., & Eliceiri, K. W. (2012). NIH Image to ImageJ: 25
1020 years of image analysis. *Nature Methods*, 9(7), 671–675. Retrieved from
1021 https://doi.org/10.1038/nmeth.2089
1022 Schoofs, A., Hückesfeld, S., Schlegel, P., Miroschnikow, A., Peters, M., Zeymer, M.,
1023 … Pankratz, M. J. (2014). Selection of Motor Programs for Suppressing Food
1024 Intake and Inducing Locomotion in the Drosophila Brain. *PLoS Biology*, 12(6).
1025 Retrieved from https://doi.org/10.1371/journal.pbio.1001893
1026 Schwarz, J. E., King, A. N., Hsu, C. T., Barber, A. F., & Sehgal, A. (2021). Hugin +
1027 neurons provide a link between sleep homeostat and circadian clock neurons.
1028 *PNAS*. Retrieved from https://doi.org/10.1073/pnas.2111183118/-
1029 /DCSupplemental
1030 Shafer, O. T., & Keene, A. C. (2021, January 11). The Regulation of Drosophila Sleep.
1031 *Current Biology*. Cell Press. Retrieved from
1032 https://doi.org/10.1016/j.cub.2020.10.082
1033 Sorribes, A., Porsteinsson, H., Arnardóttir, H., Jóhannesdóttir, I. P., Sigurgeirsson, B.,
1034 de Polavieja, G. G., & Karlsson, K. (2013). The ontogeny of sleep-wake cycles in
1035 zebrafish: A comparison to humans. *Frontiers in Neural Circuits*, 7(NOV).

Retrieved from https://doi.org/10.3389/fncir.2013.00178

Szuperak, M., Churgin, M. A., Borja, A. J., Raizen, D. M., Fang-Yen, C., & Kayser, M. S. (2018a). A sleep state in Drosophila larvae required for neural stem cell proliferation. *ELife*, 7. Retrieved 25 December 2021 from https://doi.org/10.7554/ELIFE.33220

Szuperak, M., Churgin, M. A., Borja, A. J., Raizen, D. M., Fang-Yen, C., & Kayser, M. S. (2018b). A sleep state in Drosophila larvae required for neural stem cell proliferation. *ELife*. Retrieved from https://doi.org/10.7554/eLife.33220.001

Veenstra, J. A., Agricola, H. J., & Sellami, A. (2008). Regulatory peptides in fruit fly midgut. *Cell and Tissue Research*, 334(3), 499–516. Retrieved from https://doi.org/10.1007/s00441-008-0708-3

Yoshino, J., Morikawa, R., Hasegawa, E., & Emoto, K. (2017). Neural circuitry that evokes escape behavior in response to nociceptive stimuli in *Drosophila* larvae. *Current Biology*, 27, 2499-2504.

Yoshino, J., Mali, S., Williams, C.R., Morita, T., Emerson, C., Arp, C., Miller, S., Yin, C., Motoyoshi, M., Hemmi, C., Ishii, K., Bautista, D., Emoto, K., & Parrish, J.Z. (2025). *Drosophila* epidermal cells are intrinsically mechanosensitive and modulate nociceptive behavior outputs. *ELife*, 13, PR95379 doi: 10.7554/eLife.95379

Figure 1

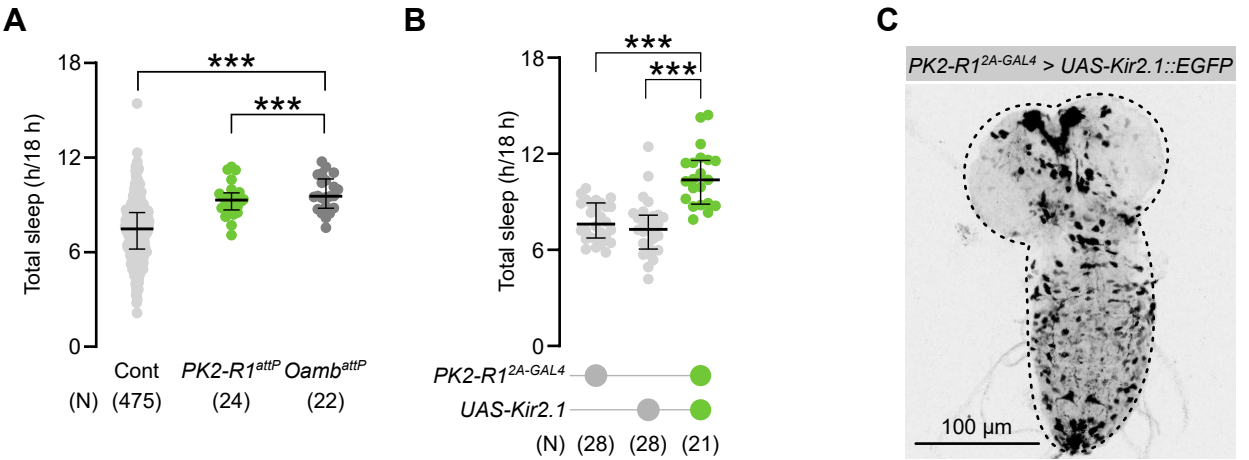
A
Total sleep (h/18 h)
18
12
6
0
***
***
Cont
PK2-R1attP
Oambattp
(N) (475)
(24)
(22)
B
Total sleep (h/18 h)
18
12
6
0
***
***
PK2-R12A-GAL4
UAS-Kir2.1
(N) (28) (28) (21)
C
PK2-R12A-GAL4 > UAS-Kir2.1::EGFP
100 µm

Figure 1—figure supplement 1

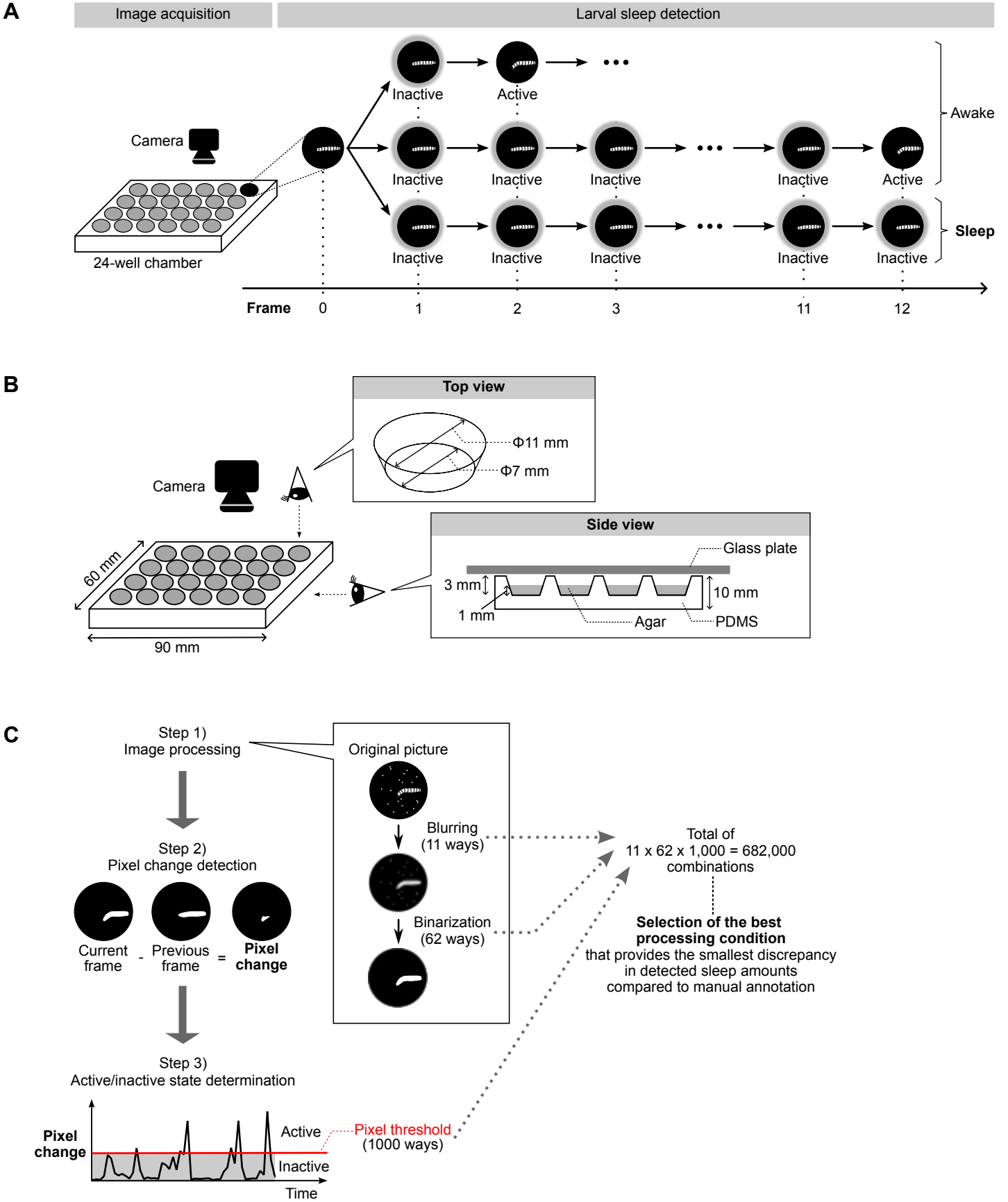

Figure 1—figure supplement 2

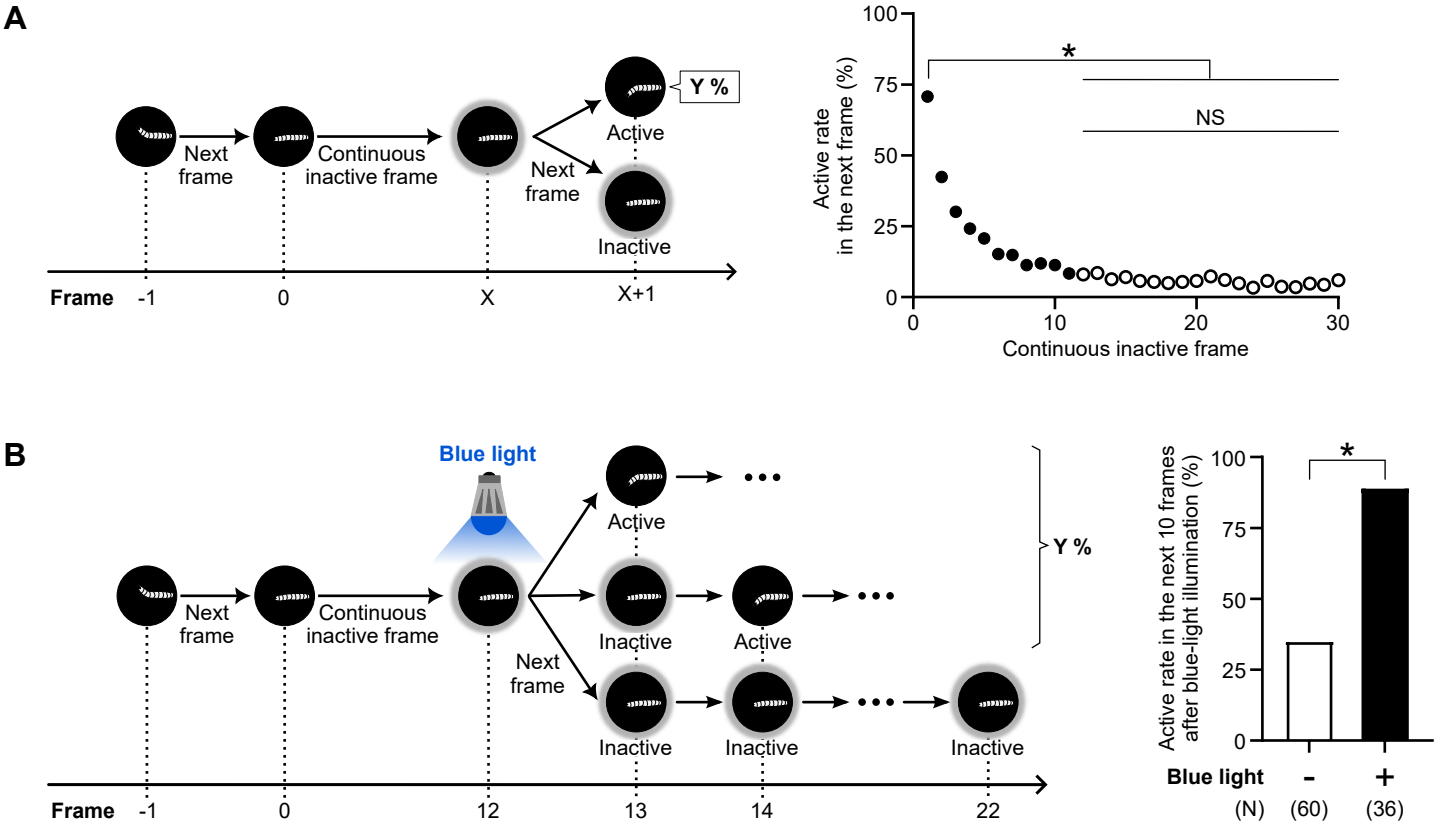

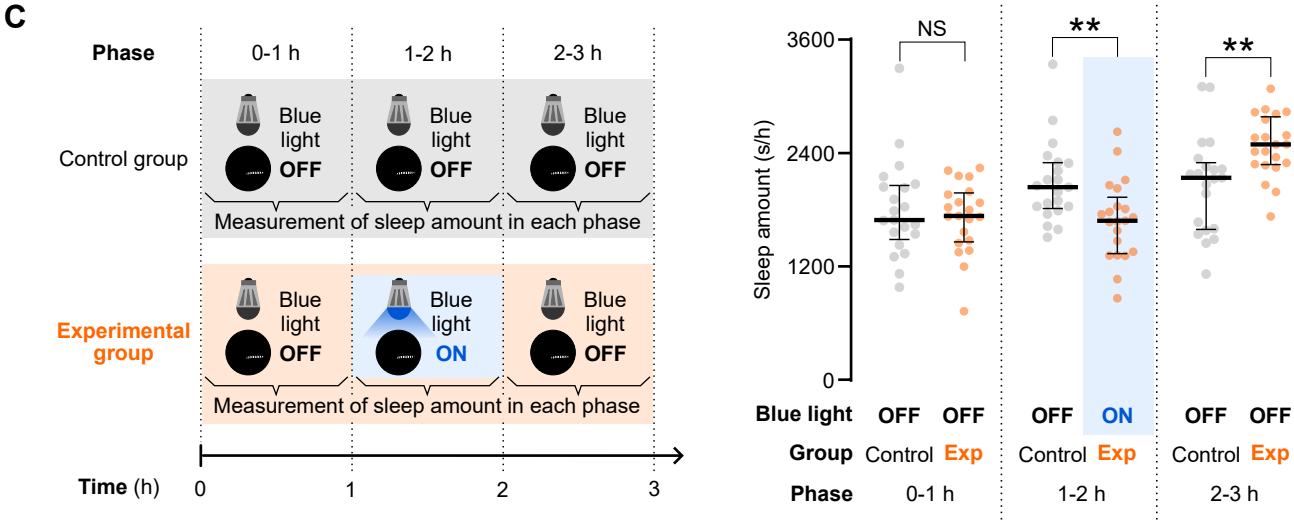

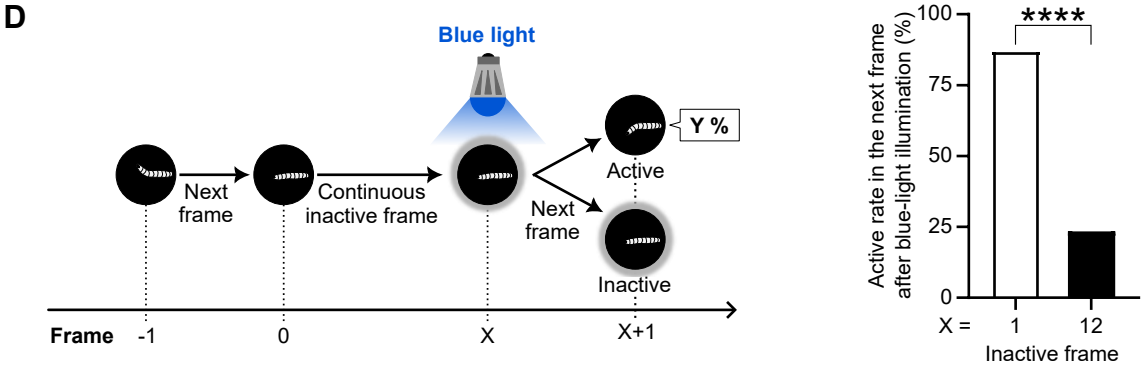

Figure 1—figure supplement 3

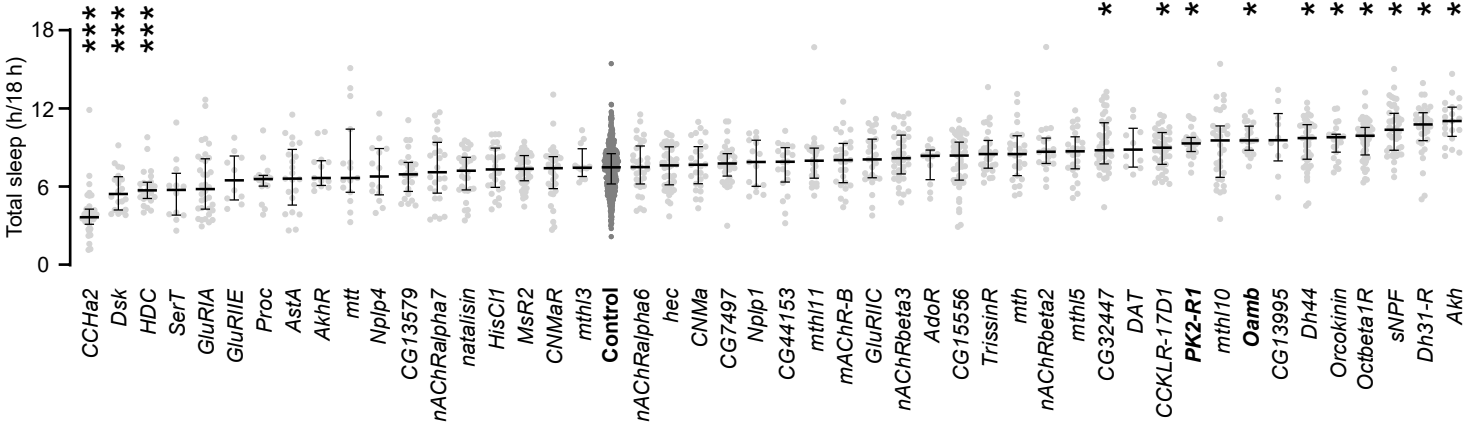

Figure 1—figure supplement 4

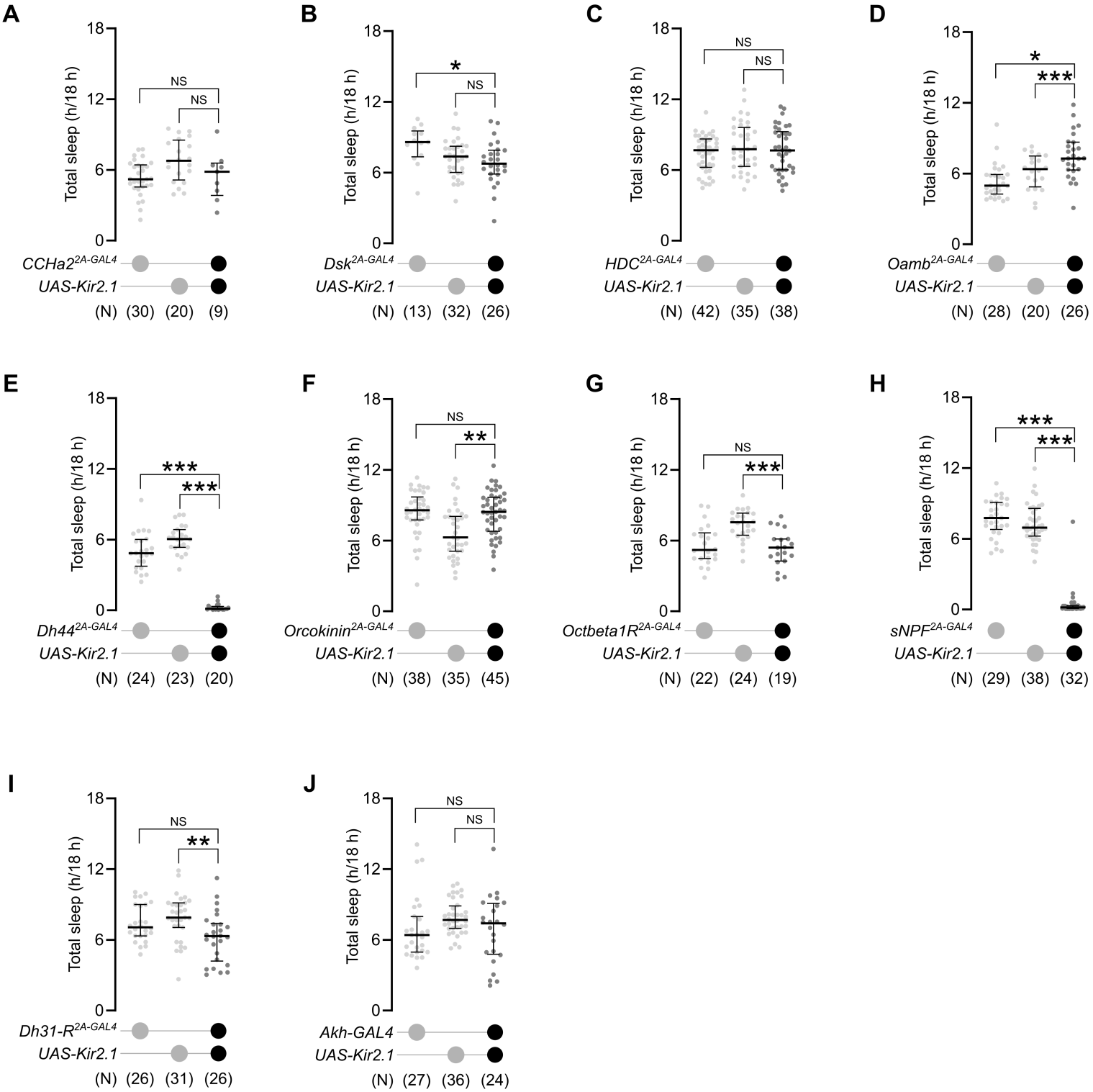

Figure 1—figure supplement 5

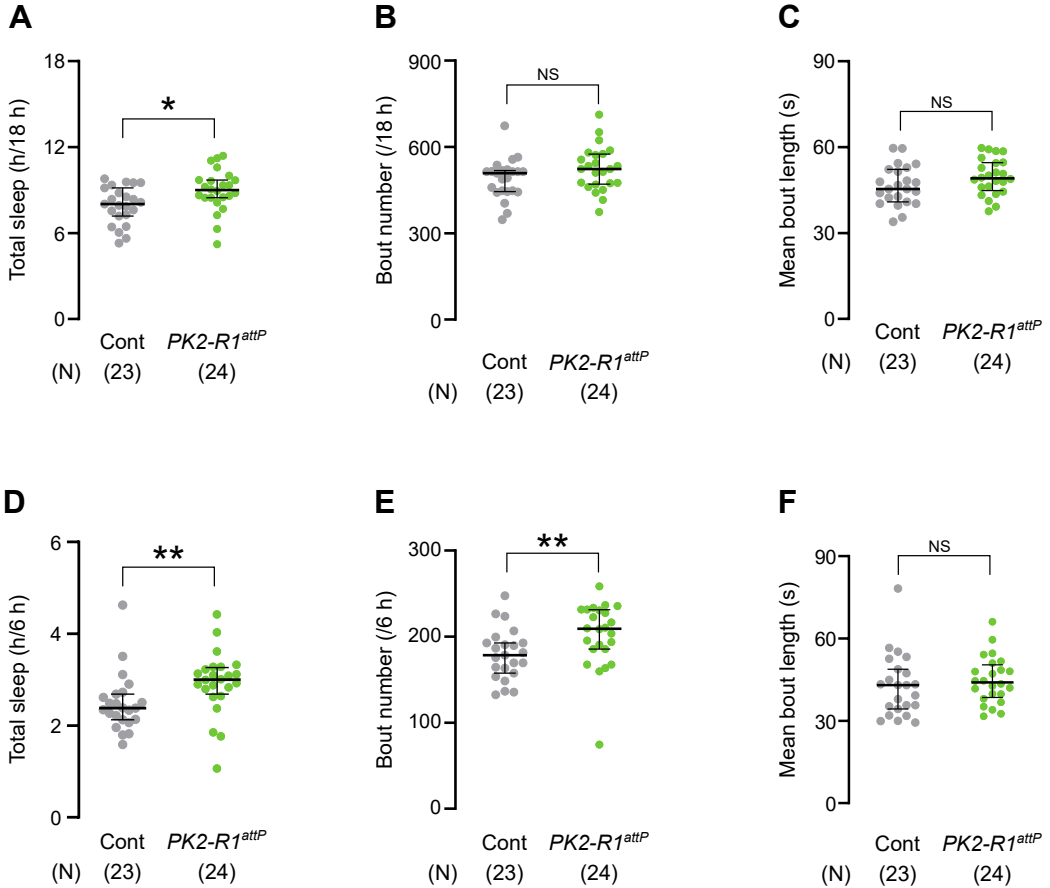

Figure 2

A

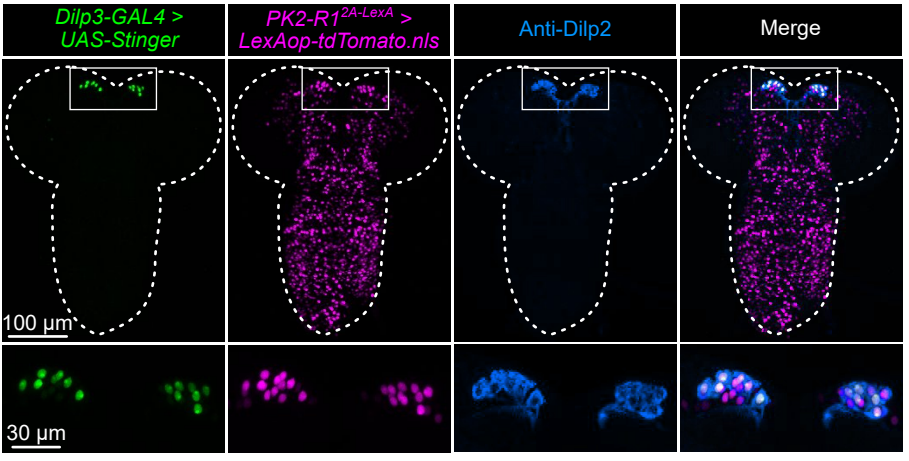

B

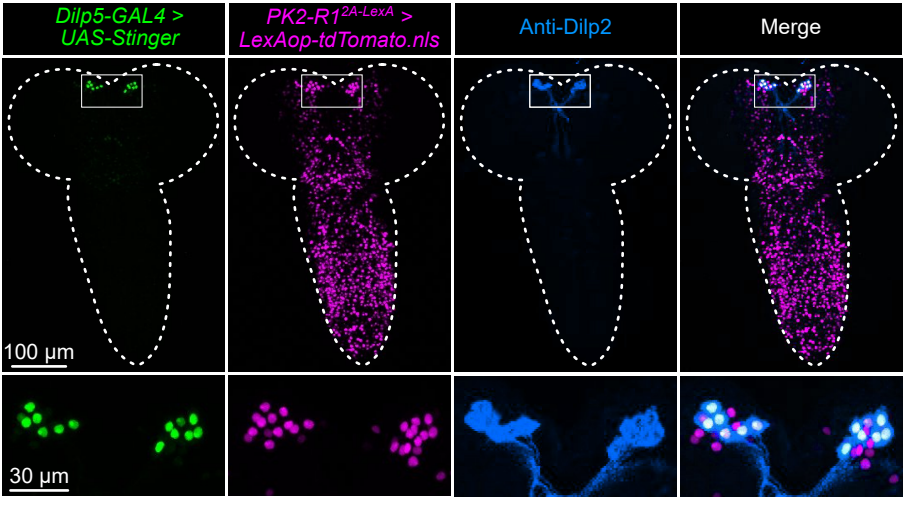

C

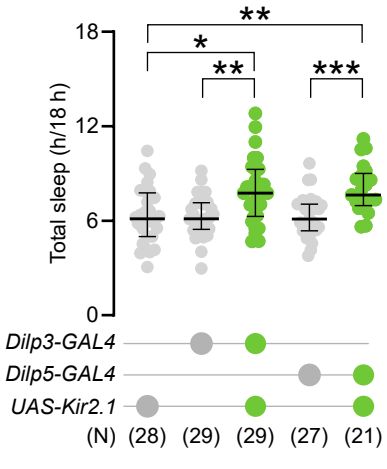

D

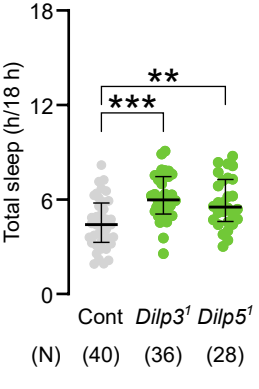

Figure 2—figure supplement 1

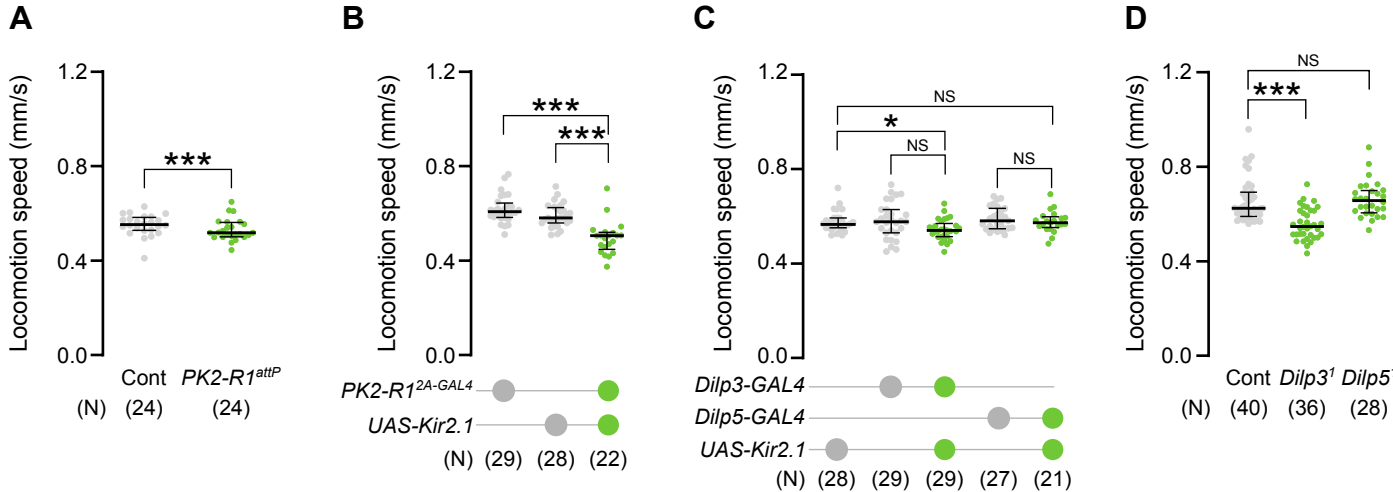

Figure 3

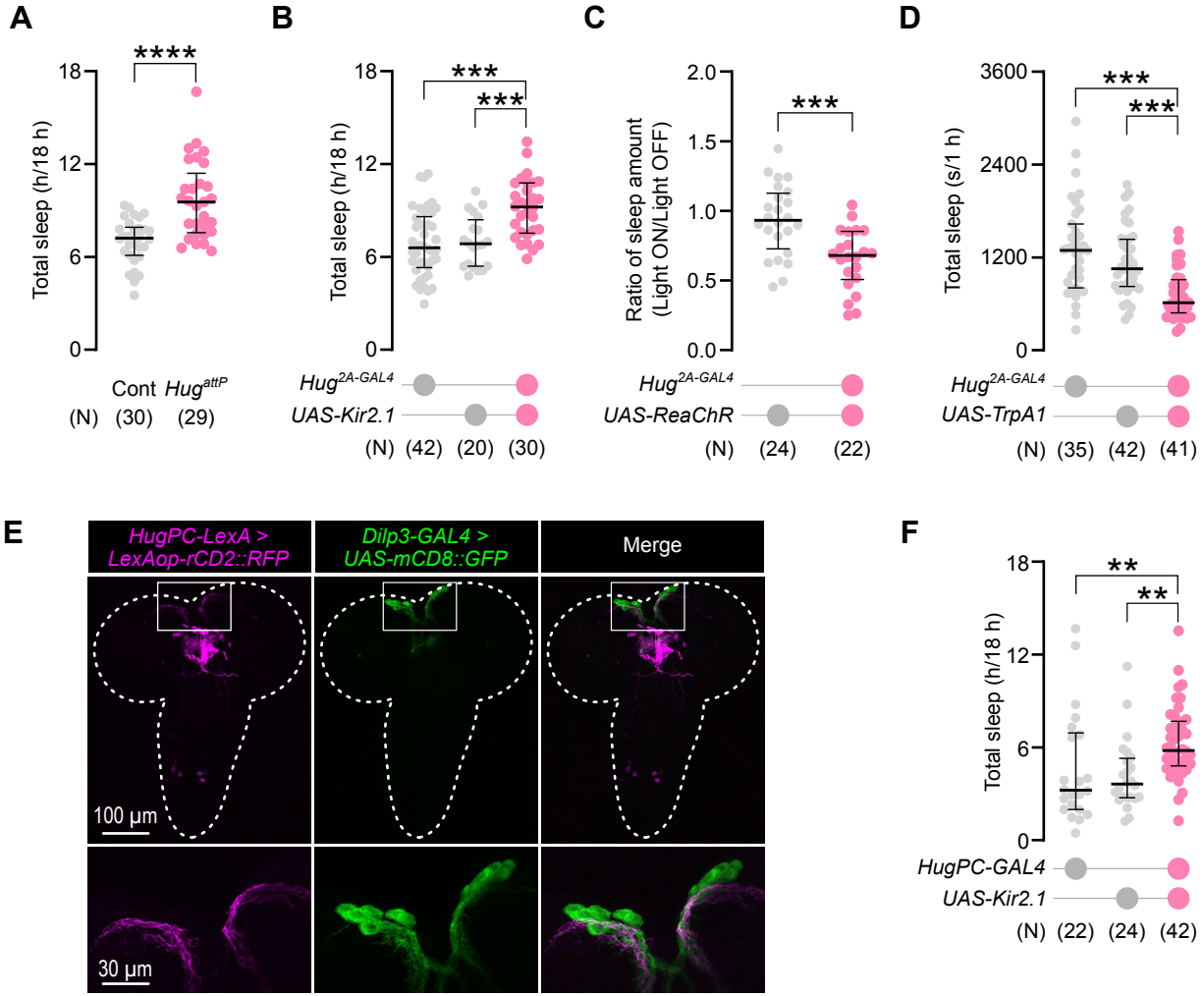
A
B
C
D
E
F
Total sleep (h/18 h)
Cont
Hug^attP
(N) (30) (29)
Hug^2A-GAL4
UAS-Kir2.1
(N) (42) (20) (30)
Ratio of sleep amount (Light ON/Light OFF)
UAS-ReaChR
(N) (24) (22)
Total sleep (s/1 h)
UAS-TrpA1
(N) (35) (42) (41)
HugPC-LexA > LexAop-rCD2::RFP
Dilp3-GAL4 > UAS-mCD8::GFP
Merge
100 µm
30 µm
HugPC-GAL4
UAS-Kir2.1
(N) (22) (24) (42)

Figure 3—figure supplement 1

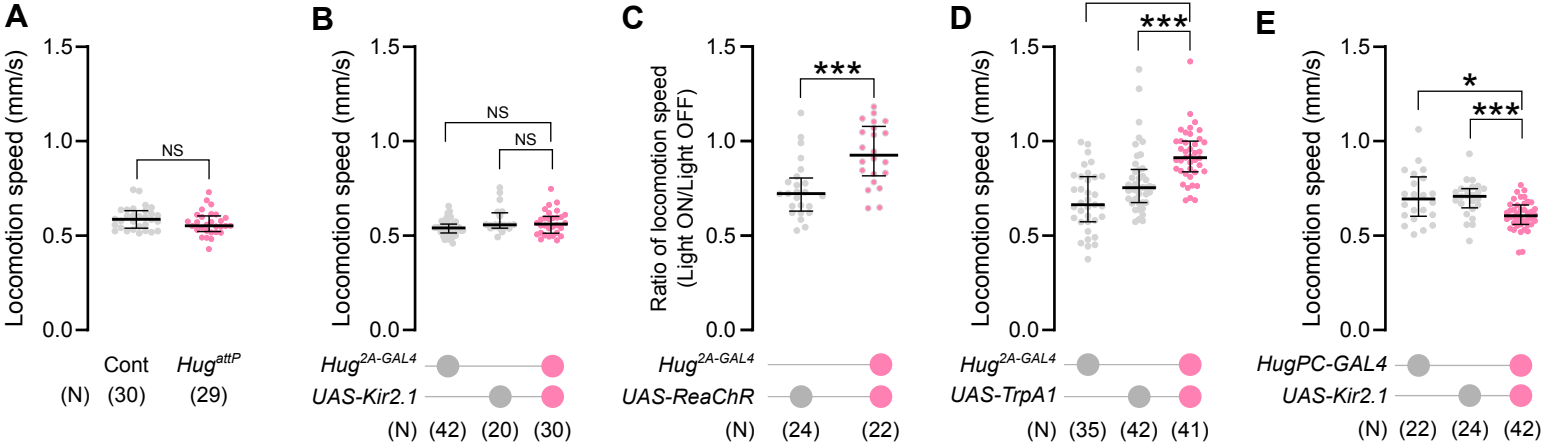

Figure 3—figure supplement 2

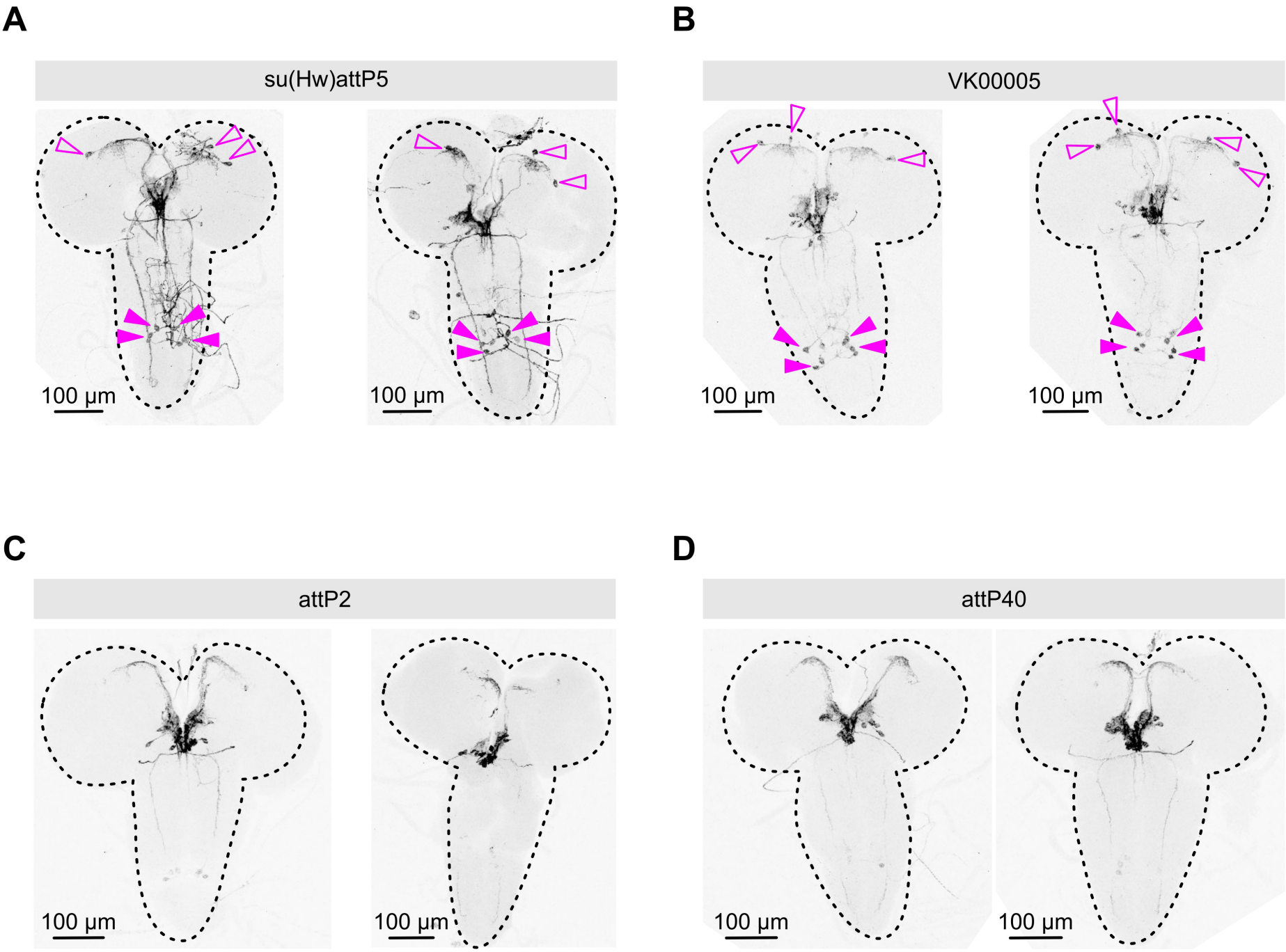

Figure 3—figure supplement 3

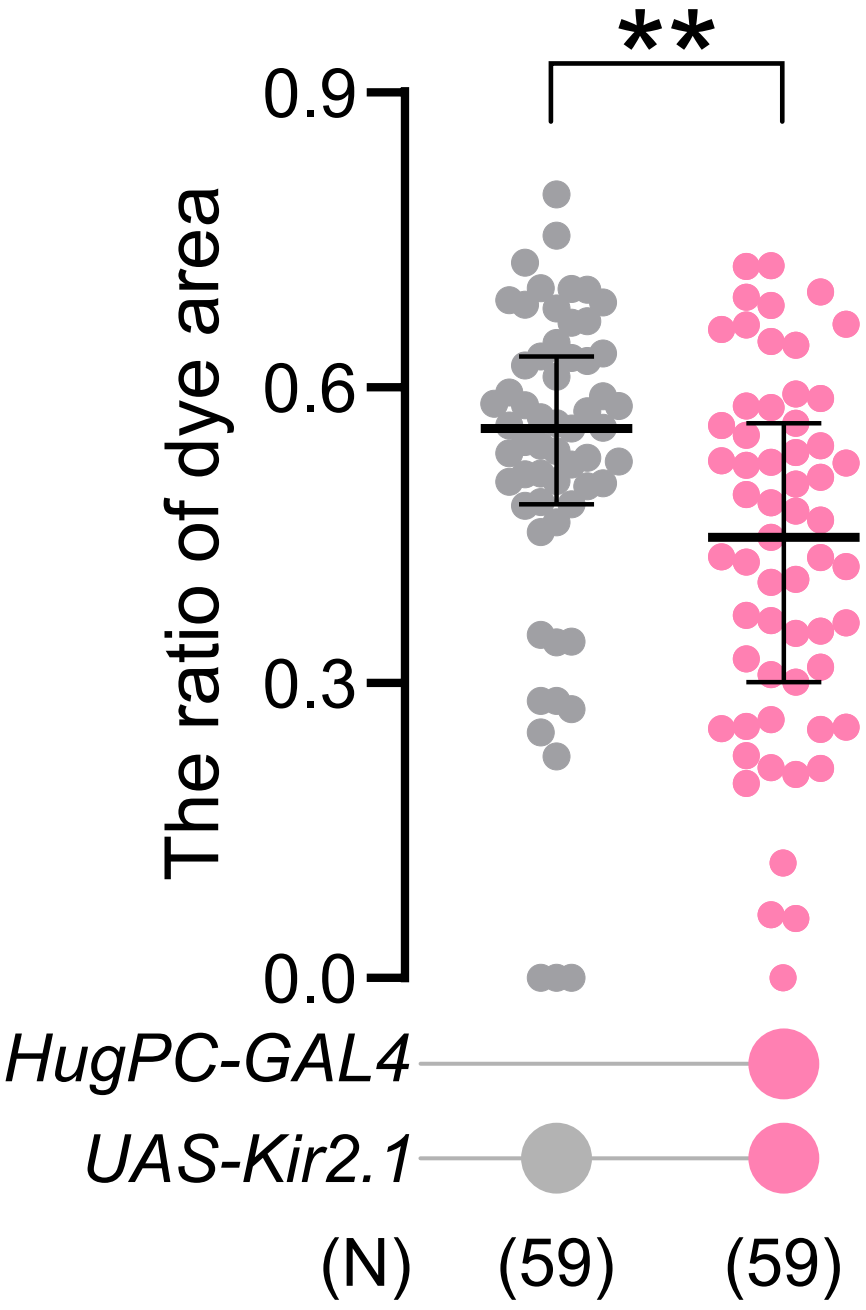

Figure 4

A

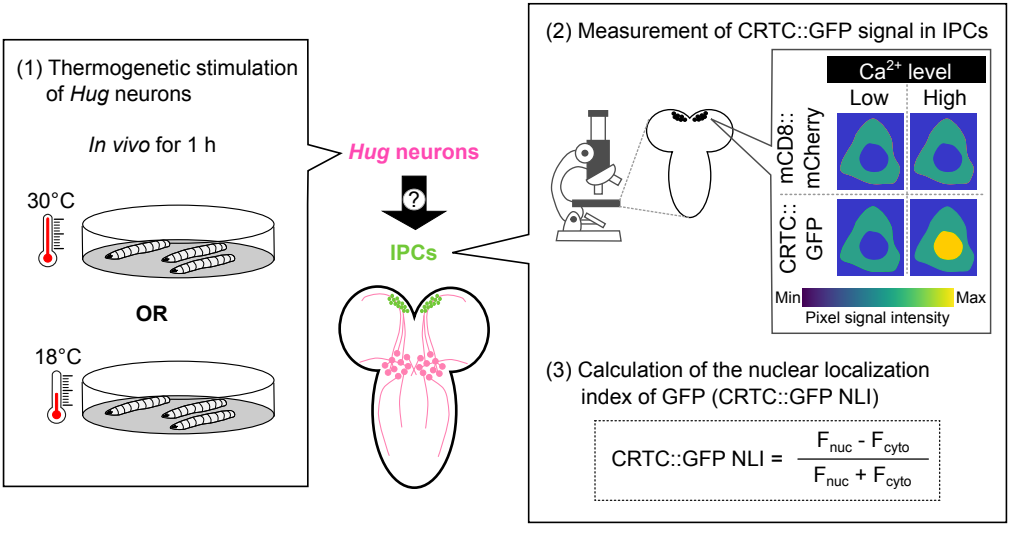

Low temperature

High temperature

B

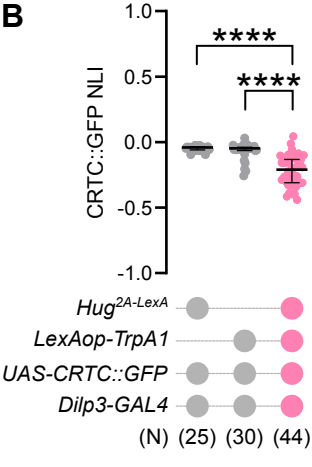

C

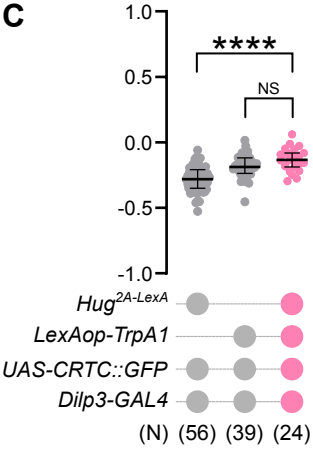

D

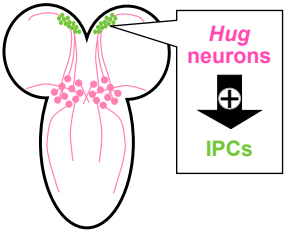

Figure 4—figure supplement 1

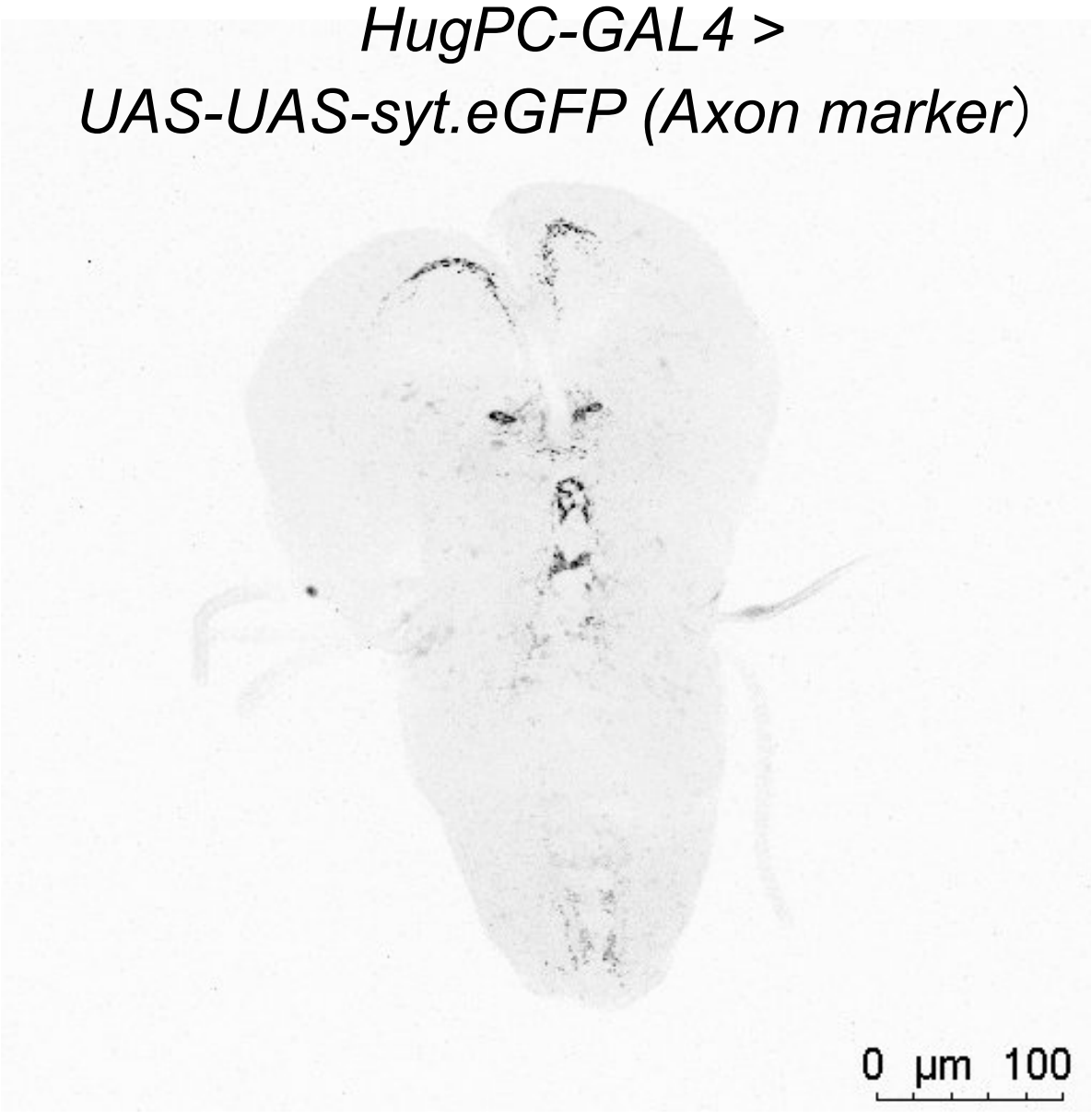

Figure 5

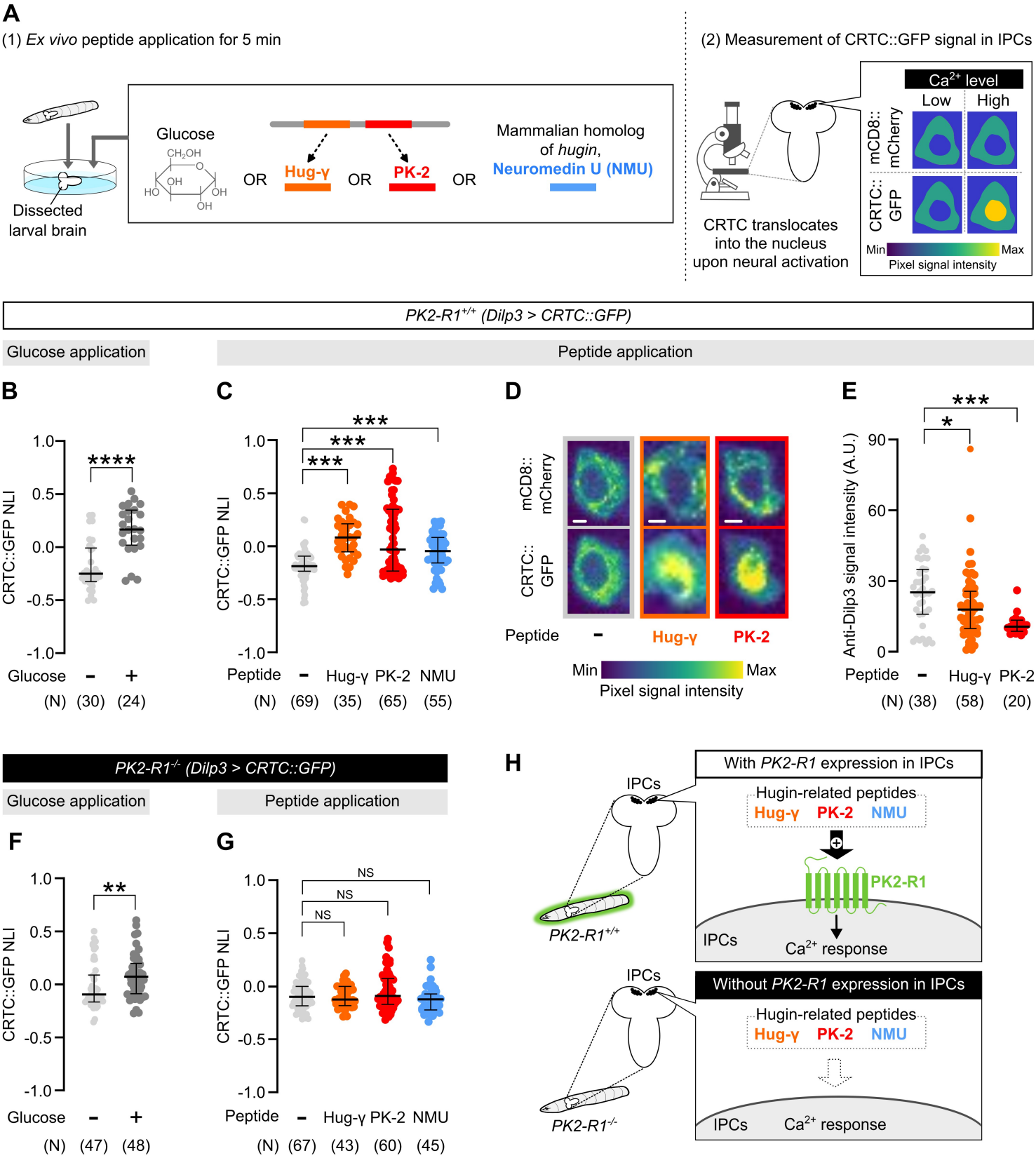
A
(1) Ex vivo peptide application for 5 min
Dissected larval brain
Glucose
CH2OH
OH
HO
OH
OH
OR
Hug-γ
OR
PK-2
OR
Mammalian homolog of hugin,
Neuromedin U (NMU)
(2) Measurement of CRTC::GFP signal in IPCs
CRTC translocates into the nucleus upon neural activation
Ca2+ level
Low
High
mCD8::mCherry
CRTC::GFP
Min
Max
Pixel signal intensity
PK2-R1+/+ (Dilp3 > CRTC::GFP)
Glucose application
Peptide application
B
CRTC::GFP NLI
1.0
0.5
0.0
-0.5
-1.0
****
Glucose - +
(N) (30) (24)
C
CRTC::GFP NLI
***
***
***
Peptide - Hug-γ PK-2 NMU
(N) (69) (35) (65) (55)
D
mCD8::mCherry
CRTC::GFP
Peptide - Hug-γ PK-2
Min
Max
Pixel signal intensity
E
Anti-Dilp3 signal intensity (A.U.)
90
60
30
0
***
*
Peptide - Hug-γ PK-2
(N) (38) (58) (20)
PK2-R1-/- (Dilp3 > CRTC::GFP)
Glucose application
Peptide application
F
CRTC::GFP NLI
**
Glucose - +
(N) (47) (48)
G
CRTC::GFP NLI
NS
NS
NS
Peptide - Hug-γ PK-2 NMU
(N) (67) (43) (60) (45)
H
IPCs
PK2-R1+/+
With PK2-R1 expression in IPCs
Hugin-related peptides
Hug-γ PK-2 NMU
PK2-R1
IPCs
Ca2+ response
IPCs
PK2-R1-/-
Without PK2-R1 expression in IPCs
Hugin-related peptides
Hug-γ PK-2 NMU
IPCs
Ca2+ response

Figure 5—figure supplement 1

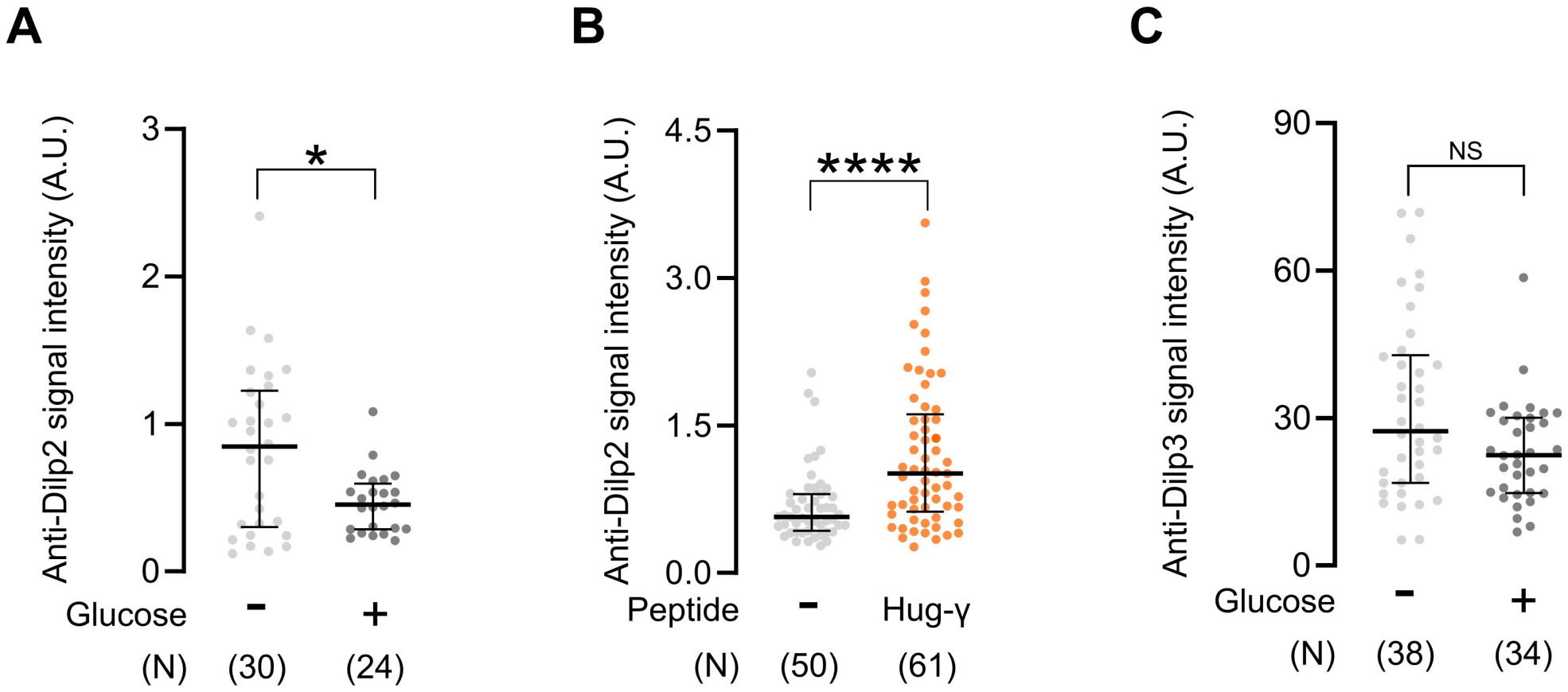

Figure 5—figure supplement 2

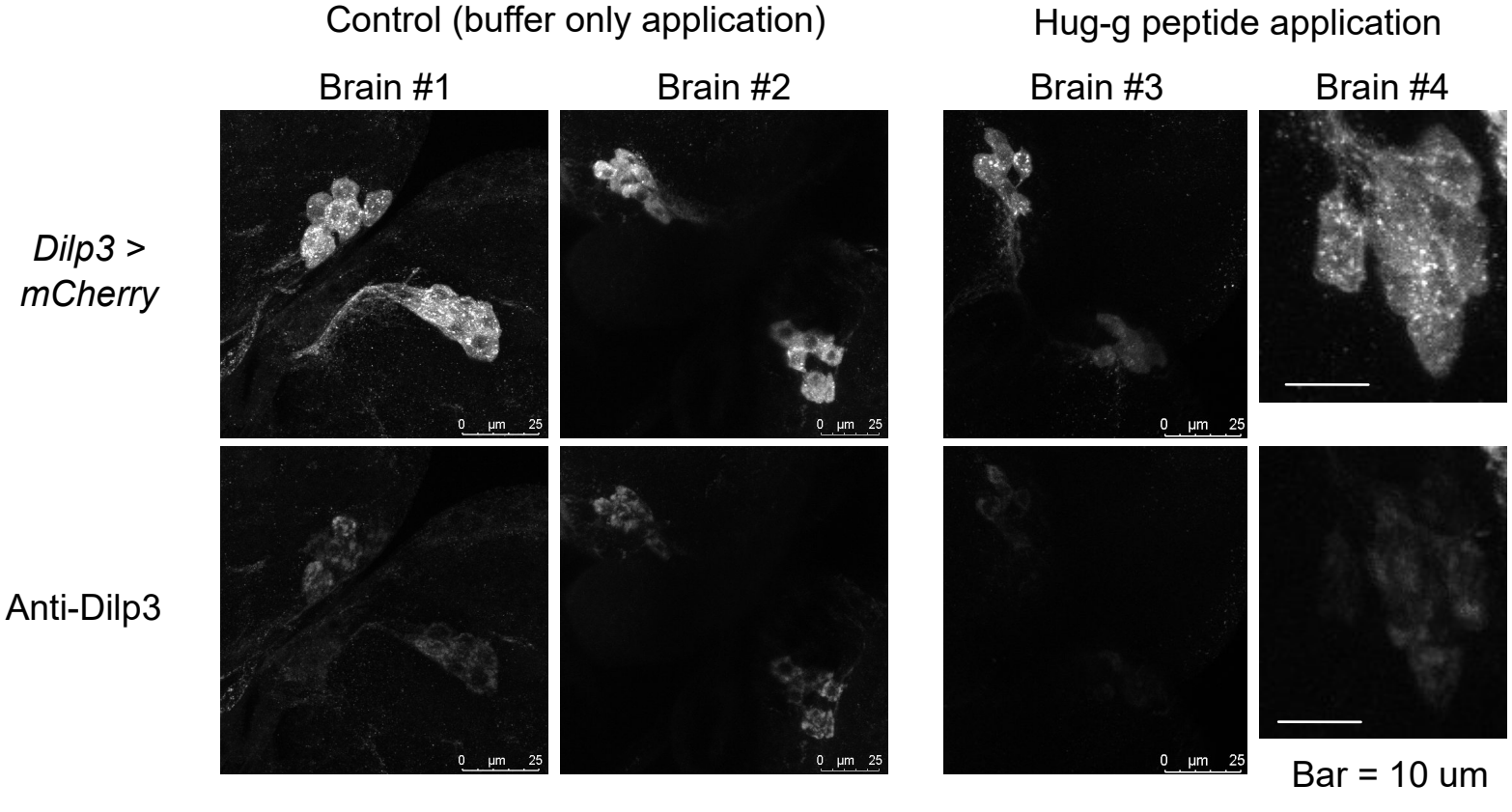

Figure 6

Sleep amount analysis

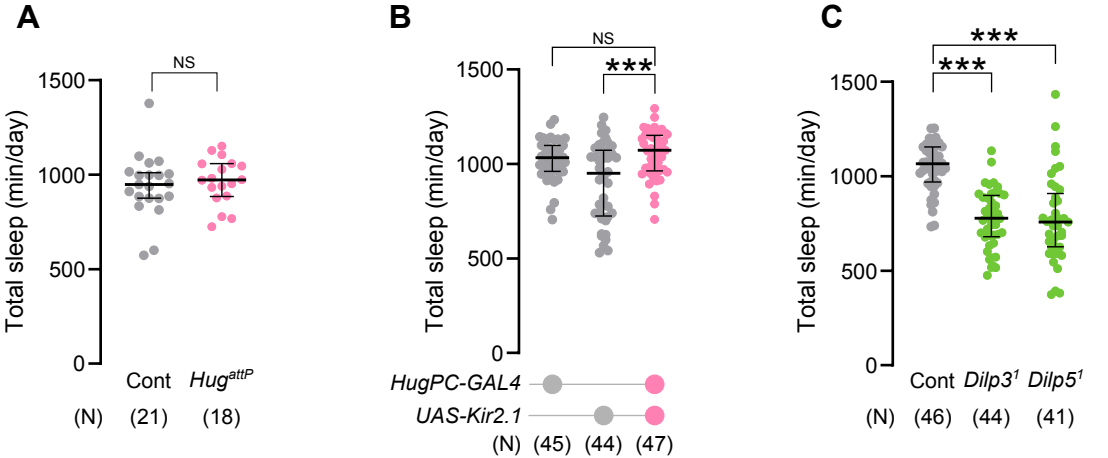

Ex vivo peptides application

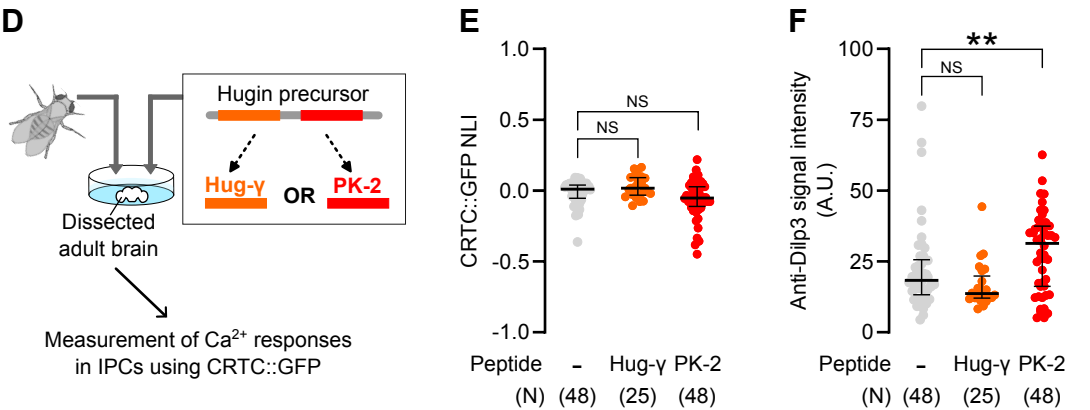

Figure 6—figure supplement 1

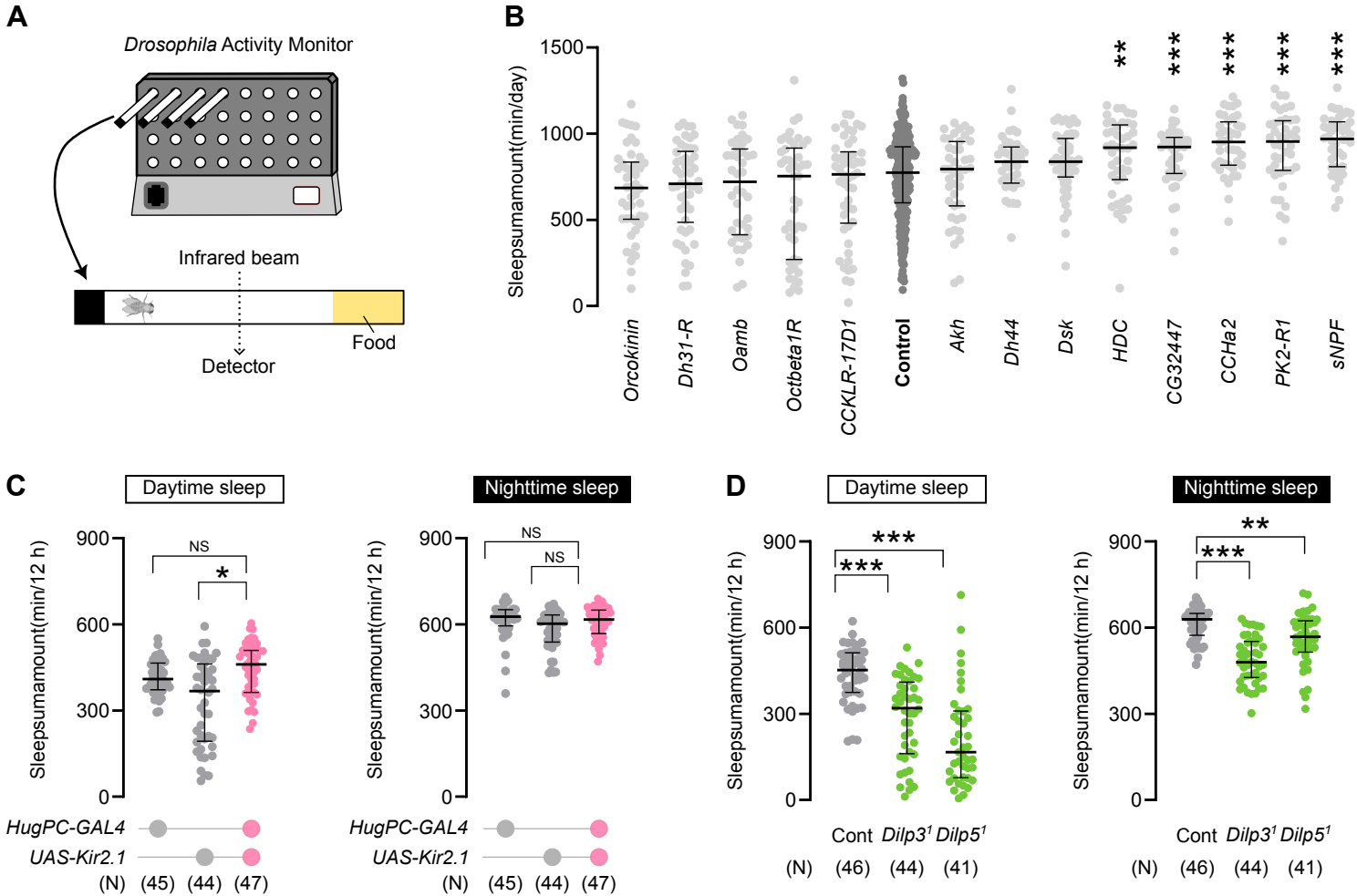

Figure 6—figure supplement 2

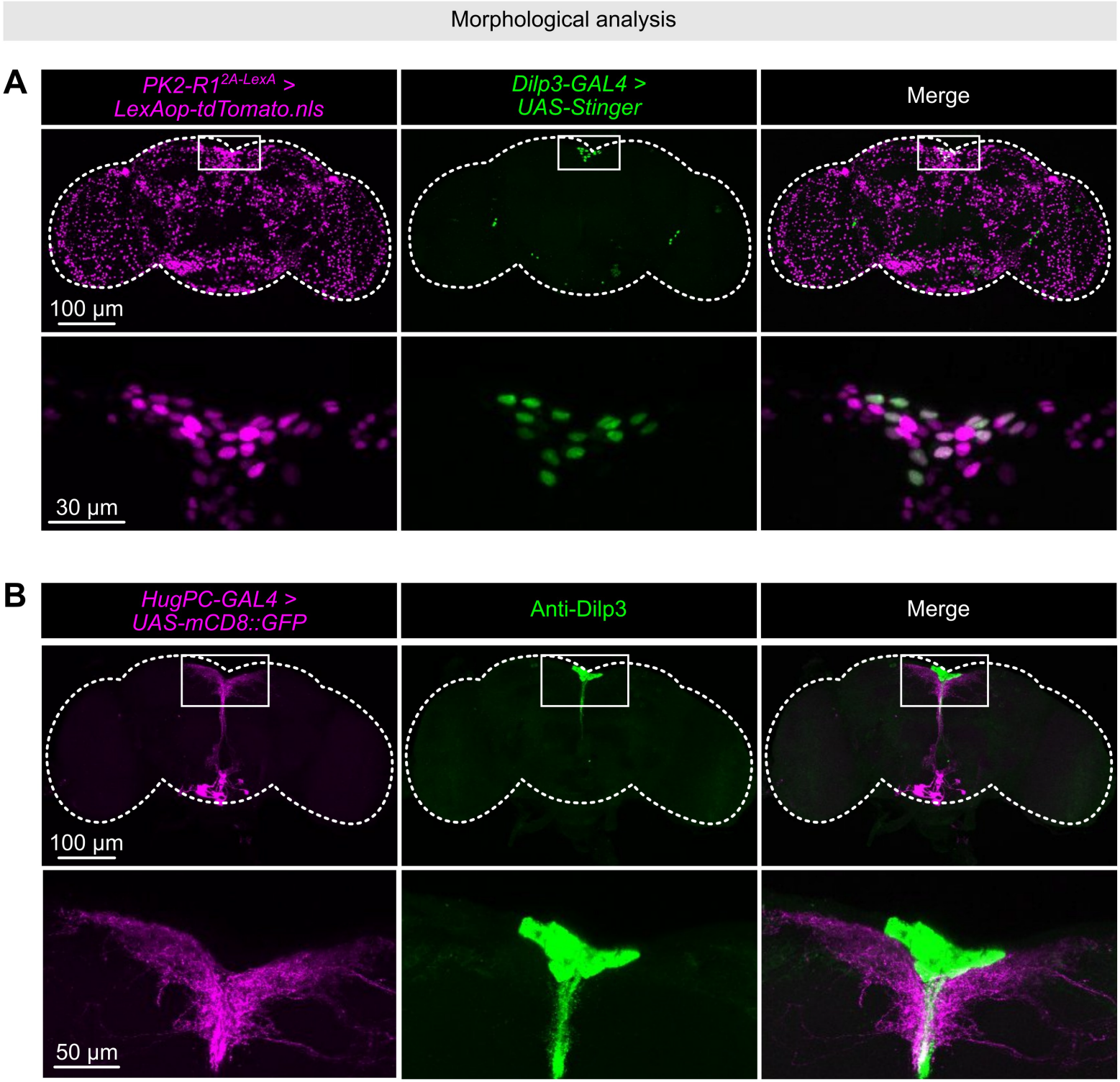

Figure 6—figure supplement 3

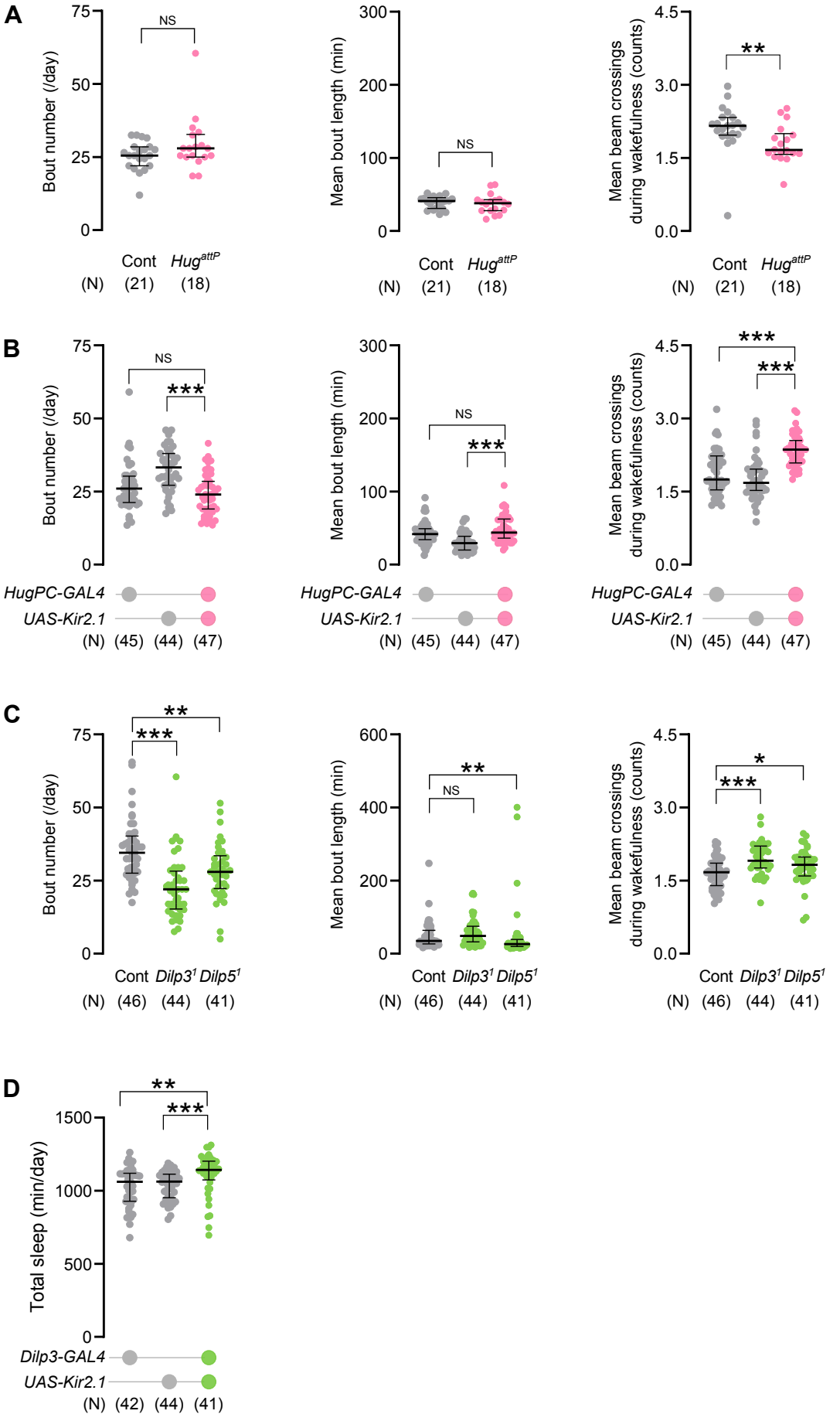

Figure 7

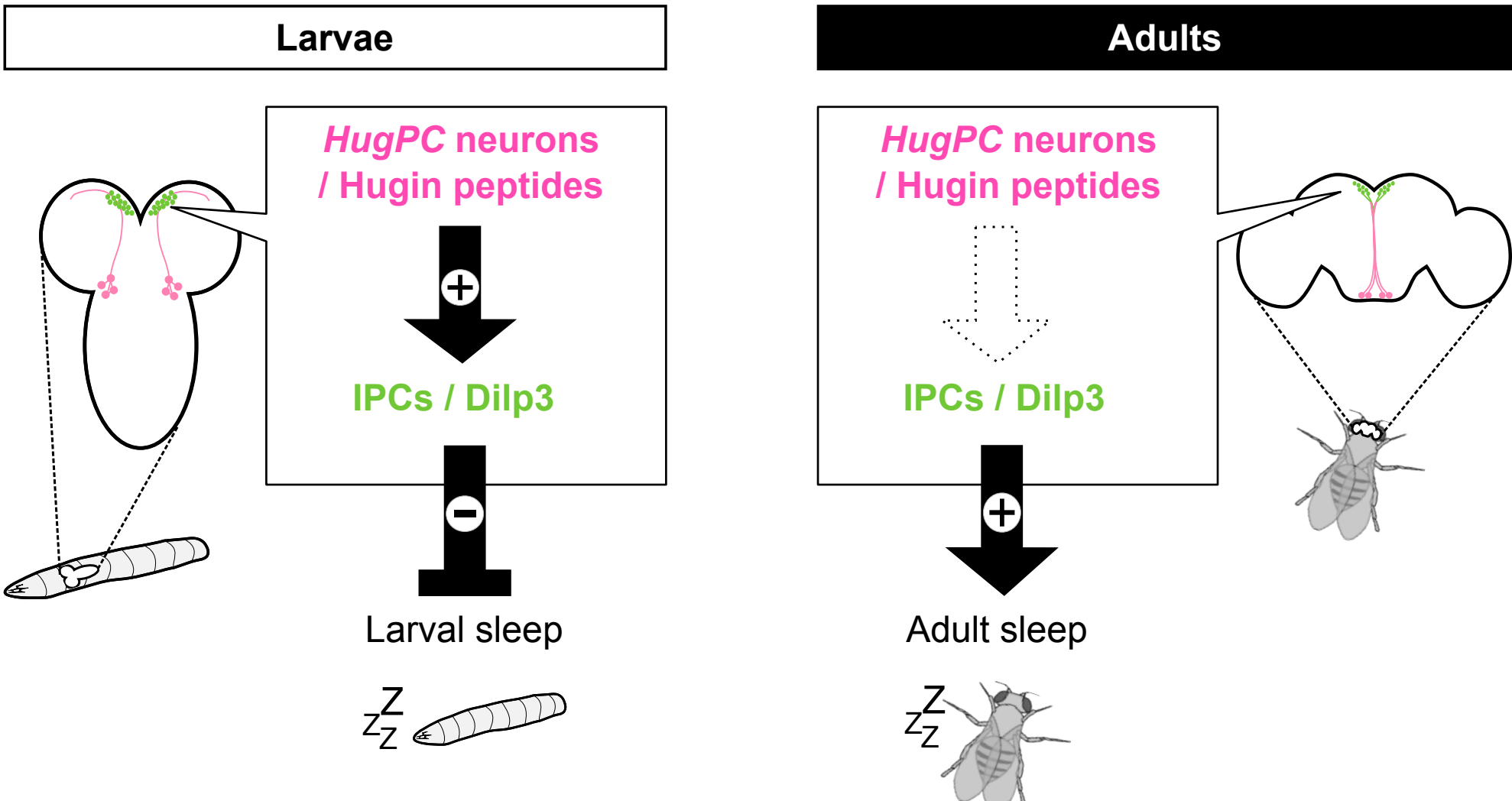
Larvae
Adults
HugPC neurons
/ Hugin peptides
IPCs / Dilp3
Larval sleep
HugPC neurons
/ Hugin peptides
IPCs / Dilp3
Adult sleep